

MULTIPLE STELLAR FORMATION EVENTS IN GLOBULAR CLUSTERS

THE IMPLICATIONS OF MULTIPLE STELLAR FORMATION
EVENTS FOR THE EVOLUTION OF GLOBULAR CLUSTERS

By

JONATHAN M.B. DOWNING, B.Sc.

A Thesis

Submitted to the School of Graduate Studies

in Partial Fulfilment of the Requirements

for the Degree

Master of Science

McMaster University

©Copyright by Jonathan Downing, July 2006

MASTER OF SCIENCE (2006)
(Department of Physics and Astronomy)

McMaster University
Hamilton, Ontario

TITLE: The Implications of Multiple Stellar Formation Events for the
Evolution of Globular Clusters

AUTHOR: Jonathan Downing, B.Sc.

SUPERVISOR: Alison Sills

NUMBER OF PAGES: xii, 92

Abstract

In this thesis we investigate the dynamical effect of a second generation of stellar formation in globular clusters in the context of the anomalous horizontal branch of NGC 2808. The horizontal branch of NGC 2808 is bifurcated in colour and exhibits an extended blue tail. This morphology can be explained if the blue tail stars have an enhanced helium content due to cluster self-enrichment. Specifically it has been proposed that NGC 2808 has experienced two distinct generations of star formation. The first generation has a top-heavy IMF, enhanced in $3 - 5M_{\odot}$ stars, and would produce many AGB stars within the first 200 Myrs of its life. The second generation then forms out of the helium-rich ejecta of the AGB stars and goes on to produce the blue tail in the horizontal branch that is currently observed in NGC 2808.

We use three types of simulations to investigate this scenario. For a control model we run a simulation with a Salpeter IMF and a single generation. We then run models with a top-heavy IMF and a single generation and models with a top-heavy IMF and two generations. In the two generation models we also investigate the effect of concentration by examining simulations with two different length scales.

We find that the models with the top-heavy IMF and a single generation are subject to extensive mass-loss in their early phases due to the large number of intermediate-mass stars and are less strongly affected by two-body relaxation than simulations with a Salpeter IMF. The models with two generations appear to be dynamically stable and long-lived objects, at least in their early stages. They seem to be observationally indistinguishable from

single-generation clusters with Salpeter IMFs on the basis of their dynamics. The stellar populations of the two-generation clusters are found to have a much higher fraction of C-O white dwarfs than clusters with a Salpeter IMF. We find no evidence that these bodies will be preferentially scattered out of the system and they should remain part of the cluster until it dissolves after core collapse. The abundance of white dwarfs would provide an observational method of identifying two generation cluster candidates.

Overall we find the two-generation scenario to be plausible on the basis of dynamics but due to the overabundance of white dwarfs produced by the top-heavy IMF and based on other studies of the chemistry of AGB stars we conclude that this scenario is unlikely to be the sole explanation for globular cluster self-enrichment.

Acknowledgements

I would like to thank my supervisor, Dr. Alison Sills, for providing me with an entirely positive experience throughout the course of my M.Sc. program. It has been a great pleasure to work with her.

I would also like to acknowledge the role tea, coffee and alcohol of all types have played in the final preparation of this thesis and during some of the dark times of hardware malfunction :)

To my mother, without whom I would not be where I am today.

Table of Contents

Abstract	iii
Acknowledgements	v
List of Figures	x
List of Tables	xii
Chapter 1 Introduction	1
1.1 Basics of Stellar Evolution	2
1.2 The Colour Magnitude Diagram	4
1.3 The Horizontal Branch	5
1.4 Asymptotic Giant Branch Stars	8
1.5 The Second Parameter Problem and the Case of NGC 2808 . .	9
1.6 Our Proposal	15
Chapter 2 Stellar Dynamics	18
2.1 Basics of N-Body Modeling	18
2.1.1 Thermo-statistics	19
2.1.2 Fokker-Planck Methods	21
2.1.3 Direct N-body Simulations	22
2.2 Explicit Behavior of N-body Systems	24
2.2.1 Scales and Diagnostics	25

2.2.2	Initial Conditions	26
2.2.3	The Case of Equal Masses	28
2.2.4	Initial Mass Functions	29
2.2.5	Stellar Evolution	30
Chapter 3 Numerical Tools		41
3.1	STARLAB	41
3.1.1	Kira	42
3.1.2	SeBa	45
3.1.3	Our Modifications	47
3.2	GRAPE	50
Chapter 4 Method		54
4.1	Choice of IMF Parameters	54
4.2	The Evolution of the First Generation	55
4.3	The Second Generation	59
4.4	Evolution of the Combined Cluster	60
4.5	Our Models	62
Chapter 5 Results		64
5.1	The Top-heavy IMF (SP vs. DC)	64
5.1.1	Dynamics	65

5.1.2	Stellar Population	69
5.2	The Second Generation (Ca5, Cb5 and Cc5)	71
5.2.1	Dynamics	71
5.2.2	Stellar Populations	76
5.3	The Effect of Length (C2.5)	78
Chapter 6 Discussion and Conclusions		83
6.1	Discussion of Results	83
6.2	Observational Prospects	86
6.3	Prospects for AGB Stars in the Self-enrichment Scenario . . .	87
6.4	Conclusion	89

List of Figures

1.1	Canonical Horizontal Branch	6
1.2	CMD for NGC 2808	12
2.1	Lagrangian Radii for Equal Masses	32
2.2	Our Lagrangian Radii for Equal Masses	33
2.3	Mass segregation	34
2.4	Our result for mass segregation	35
2.5	The Effects of Stellar Evolution	36
2.6	Number dependence of stellar evolution effects	37
2.7	Our stellar evolution results	38
3.1	Starlab tree structure	42
3.2	D’Antona and Caloi mass function	49
3.3	Mass function sanity check	50
4.1	The effect of a Plummer potential	58
5.1	Lagrangian radii	66
5.2	RMS velocities	66
5.3	Average masses	67
5.4	IMF evolution	70

5.5	Lagrangian radii - 2^{nd} generation	73
5.6	RMS velocity - 2^{nd} generation	74
5.7	Average masses - 2^{nd} generation	75
5.8	IMF evolution - 2^{nd} generation	77
5.9	Dynamical properties - 2.5 pc length scale	81

List of Tables

4.1	Simulation Parameters	62
5.1	Physical parameters	65
5.2	Stellar populations	69
5.3	Physical parameters - 2^{nd} generation	71
5.4	Stellar populations - 2^{nd} generation	79
5.5	Physical parameters - 2.5 pc length scale	79
5.6	Stellar population - 2.5 pc length scale	82

Chapter 1

Introduction

Globular clusters are gravitationally bound collections of stars, typically including between 10^3 and 10^7 members, which normally occur within the halos of galaxies. Galactic globular clusters are understood to be old objects, up to 12 Gyr in age and are thus primordial components of the galaxy. Conventionally all stars within a globular cluster are thought to have formed at the same time and out of the same medium, and thus share the same age and chemical composition. In particular all stars in a given globular cluster tend to have the same $[Fe/H]$ (logarithmic iron to hydrogen fraction relative to the solar abundance) value and are said to be mono-metallic. The only differentiation between stars in this scenario is their spectrum of masses determined by an initial mass function (IMF). There is thought to be a universal IMF for all globular clusters but there is some debate as to its exact form (Kroupa (2002) and references therein).

Although this description works well for the most part, several globular clusters display population characteristics that are inconsistent with this model. In many clusters all stars have the same $[Fe/H]$ but there are star-to-star abundances variations in other elements. In particular many globu-

lar clusters stars show strong star-to star O-Na and Mg-Al anticorrelations. Some clusters also display peculiar morphologies in the horizontal branch of the Colour-Magnitude Diagram (see Section 1.2). In some cases two different clusters with the same $[Fe/H]$ and with otherwise identical colour-magnitude diagrams will have differing horizontal branch morphologies. Such clusters seem to require a second parameter (other than metallicity) in order to explain the variations between them. In other cases the morphology of the horizontal branch within a single cluster cannot be explained solely by the IMF. The galactic globular cluster NGC 2808 is a particular example of this and will be discussed in detail in Section 1.5. One possible source of these anomalies is a self-enrichment scenario where chemicals produced by some cluster stars are incorporated into other cluster stars which then display abundance anomalies. The variation of the self-enrichment scenario in which we are the most interested is the production of excess helium by asymptotic giant branch (AGB) stars because this scenario could produce the anomalous horizontal branch of NGC 2808. In order to discuss this problem the basics of stellar evolution and in particular the nature of horizontal branch and asymptotic giant branch (AGB) stars must be understood.

1.1 Basics of Stellar Evolution

It is important to note that the exact course stellar evolution takes is primarily determined by the mass of the star involved. This basic review will concentrate on stars of mass $< 5M_{\odot}$ since these are the stars of most interest in the context of this problem. In this section an overview of all stages of

stellar evolution is given. Details of horizontal branch (HB) stars and AGB stars will be given in Sections 1.3 and 1.4 respectively.

A star starts its life as part of a cloud of molecular gas. As density perturbations form, the cloud starts to fragment and collapse. The central parts of the collapsed regions eventually reach sufficient densities that deuterium and hydrogen start to fuse. It is at this point that a star is considered to have formed. Once a star starts fusing hydrogen into helium in its core it enters the main sequence phase of its life. This is the longest phase of stellar evolution, typically occupying some 80% to 90% of the life of the star. The sun is a prototypical main sequence star. Eventually the hydrogen fraction in the core of the star will be reduced sufficiently that hydrogen burning in the core will shut down but continue in a thick shell around the now predominantly helium core. The star has now entered the red giant branch (RGB) phase of its life. During the RGB phase the hydrogen-burning shell will get progressively thinner and hotter which in turn will cause the envelope around the shell to expand. Overall the star will become progressively brighter but its effective temperature will decrease. During this phase material from the hydrogen burning shell can become mixed with the convective envelope in an event known as the first dredge-up. This phase is also associated with stellar-wind driven mass-loss from the envelope. Eventually the core will contract sufficiently that helium burning can commence. The star now moves on to the horizontal branch phase of its life. This phase is characterized by a hydrogen burning shell over a helium burning core. The position of a star on the horizontal branch is determined by the mass and composition of its envelope (core masses and compositions are similar across the HB). When the helium in the core is exhausted the star

will start burning helium in a shell around a primarily carbon-oxygen core and will continue burning hydrogen in an outer shell around the helium shell. This is called the asymptotic giant branch (AGB) phase of stellar evolution and it is characterized by stellar pulsations and extensive mass-loss through stellar winds. Second and even third dredge-up events can occur during the AGB stage. Ultimately for a star $< 4M_{\odot}$ the winds will remove the entire outer envelope leaving the electron-degenerate carbon-oxygen core surrounded by very thin layers of hydrogen and helium (the remnant core is called a white dwarf (WD)) surrounded by a cloud of former envelope material known as a planetary nebula. For stars between $4M_{\odot}$ and $8M_{\odot}$ the carbon-oxygen core may ignite explosively and blow apart the entire star in a supernova, leaving only a planetary nebula behind. For stars above $8M_{\odot}$ the carbon-oxygen core can undergo further fusion reactions producing elements such as silicon, nickel and eventually iron. These stars will finally undergo a supernovae, leaving behind a compact remnant (either a neutron star or a black hole).

1.2 The Colour Magnitude Diagram

The CMD (known to theorists as the Hertzsprung-Russell Diagram) is intimately associated with stellar evolution. It plots the magnitude (intrinsic brightness) of a star on the vertical axis (smaller numbers mean brighter stars) versus what astronomers call colour (essentially the difference between magnitudes for the same star taken in different wavelength regions) on the horizontal axis. The objects on the left side of the CMD are called blue and on the right side of the CMD are called red. Non-trivial transformations can

be performed which allow the horizontal axis of the CMD to be read as temperature increasing from right to left. Stars occupy specific areas of the CMD depending on their age, mass, metallicity and stage of evolution. Metallicity refers to the abundance of elements heavier than hydrogen and is measured either by mass fraction, Z , or relative to the solar abundance (such as $[Fe/H]$). A CMD can be plotted at a given time for an observed or a synthetic population of stars with each star represented as a point on the CMD. Such a plot yields a great deal of information about the evolutionary state of the population. Given the assumptions about the uniform chemistry and age of globular clusters, the morphology of the CMD for a given globular cluster should be solely determined by the age of the cluster and its IMF. This is why the anomalous appearances of certain globular cluster CMDs are so surprising if the single-generation, uniform primordial medium assumption is made.

1.3 The Horizontal Branch

The horizontal branch is a horizontal locus of stars located on the middle left of the CMD of a globular cluster. A simulated example of the canonical horizontal branch for a metal-rich globular cluster (such as NGC 2808) is shown in Figure 1.1 (Sweigart & Catelan, 1998).

The progenitors of horizontal branch stars are RGB stars and there are two mechanisms by which stars move to the horizontal branch, both involving helium ignition in the core. For stars with a mass $> 2M_{\odot}$ during the RGB phase, the hydrogen burning shell dumps helium onto the core and becomes thinner. At some point the core becomes sufficiently hot and dense ($\sim 1.3 \times$

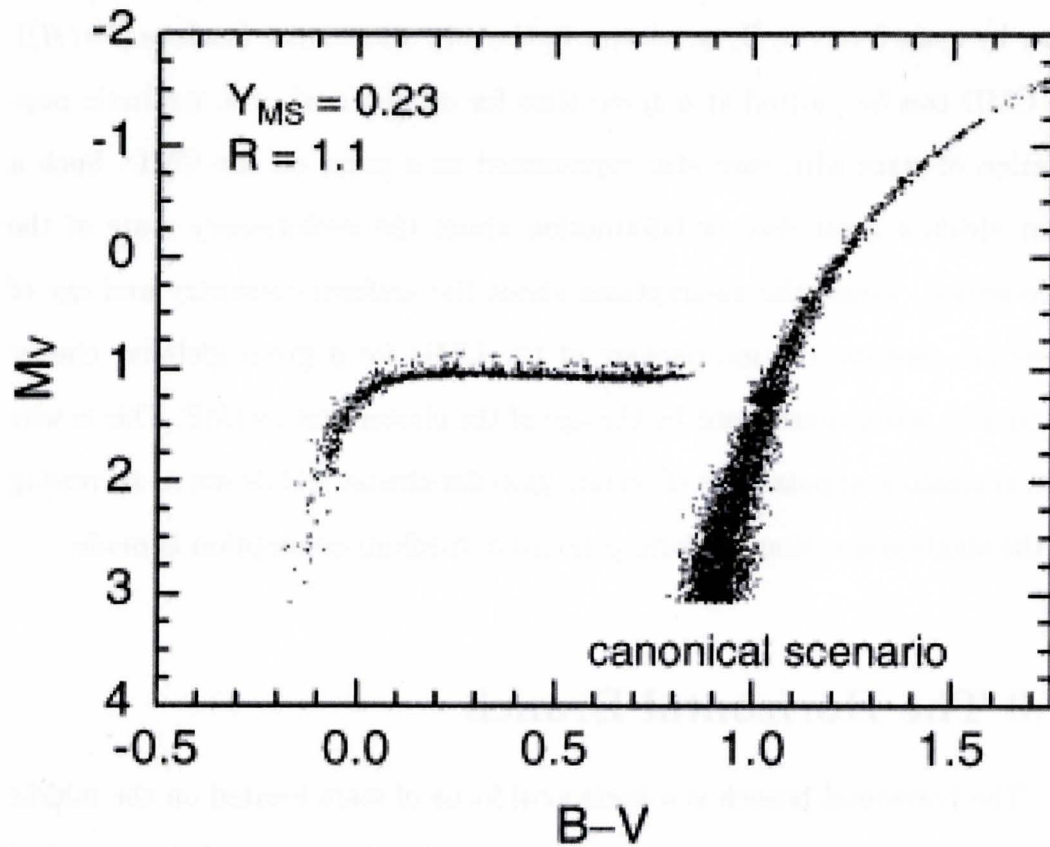


Figure 1.1 A simulation showing the canonical horizontal branch morphology for a metal-rich globular cluster ($Y_{MS} = 0.23$, $Z = 0.006$). The spread in the horizontal branch is due mainly to different envelope masses resulting from varying mass-loss during the previous RGB phase of stellar evolution. R refers to the ratio between HB stars and RGB stars brighter than the mean RR Lyrae luminosity (Sweigart & Catelan, 1998).

$10^8 K$ and $\sim 7.7 \times 10^3 g/cm^3$) that the helium nuclei can tunnel through the Coulomb barrier and start fusing into carbon via the triple- α process. The ignition is fairly gentle in this case and the star moves onto the horizontal branch quietly. If the star has a mass $< 2M_{\odot}$ the helium core is able to collapse further and becomes electron-degenerate (reaching temperatures of $10^8 K$ and densities of $10^4 g/cm^3$). Electron degeneracy pressure is essentially independent of temperature and the electron degeneracy must be lifted before the core can expand, the temperature decrease, and the core stabilize. Since the triple- α process has a very strong temperature-dependence the higher temperatures in this scenario produce an explosive ignition of helium in the core (releasing some $10^{11} L_{\odot}$). This violent ignition is called the helium flash and is very different from the ignition in the more massive stars. The flash is inferred rather than observed since most of the energy goes to lifting the electron-degeneracy in the core and the rest is absorbed by the envelope.

As afore mentioned, the stars on the horizontal branch are characterized by a hydrogen burning shell surrounding a helium burning core (as a rule of thumb the stars on the left side of the CMD are core burning while the stars on the right side are shell burning). The progenitors of HB stars are RGB stars. The position of a star on the horizontal branch is determined by the mass of the envelope (the He burning cores tend to be of the same mass across the HB) with the lower masses tending towards the blue end of the horizontal branch and the higher masses tending towards the red (de Boer, 1999). The variation in mass is largely due to varying mass-loss rates in the RGB phase. At current globular cluster ages ($\sim 10 - 12$ Gyr) a star entering the RGB will have a mass of $\sim 0.8M_{\odot}$ (monotonically increasing with lookback time) and leave

with a mass of $\sim 0.5 - 0.7M_{\odot}$. This produces a similar range of masses (at least initially) on the horizontal branch. Metallicity is also known to have an effect on horizontal branch morphology with lower metallicity clusters tending to be more populated at the blue end. These factors lead to the expectation that globular clusters with the same age and metallicity (which essentially traces the chemical composition of the clusters) would have similar horizontal branches.

It is also possible for stars on the horizontal branch to develop instabilities in their envelopes. This can lead to stellar pulsations and variability in brightness. Such stars are either RR-Lyrae variables or, if more massive, Cepheid variables. Cepheid variables in particular have a well-defined relationship between magnitude and frequency of pulsation and are important to observers as standard candles.

1.4 Asymptotic Giant Branch Stars

AGB stars are characterized by concentric hydrogen and helium-burning shells surrounding an inert carbon-oxygen core with a temperature of $\sim 2 \times 10^8 K$ and a density of $\sim 10^6 g/cm^3$. These shells are surrounded by a non-burning envelope consisting primarily of hydrogen and helium with traces of other heavier elements. The hydrogen and helium shells interact with each other when the hydrogen-burning shell dumps helium into the helium-burning shell. The helium shell gains mass and ignites causing the hydrogen shell to expand, cool and stop burning. Without a source of additional helium the helium shell stops burning and contracts causing the hydrogen shell to contract

and ignite again. This cycle causes stellar pulsations and leads to another class of variable stars, the long period variables. During the AGB phase the constant pulsations of the burning shells cause mixing at the shell boundaries and the envelope becomes further enriched with heavy elements from the stellar interior. These events are known as the second and third dredge-up. As well as producing more helium there are other cycles at work in AGB stars that produce and destroy other elements. In particular the CNO cycle operates in cooler phases while Ne-Na and Al-Mg cycles occur at higher temperatures. These cycles produce or destroy the involved elements and further change the composition of the envelope of the star. It is important to note that AGB stars do not produce iron so the iron abundance is left unchanged in these objects. AGB stars also experience extensive mass-loss and lose most of their envelopes to stellar winds. The material ejected in this way reflects the composition of the AGB envelope and can enrich the interstellar medium (ISM) in AGB-produced elements (particularly helium). This enrichment process *may* be significant for the evolution of later generations of stars in globular clusters through the self-enrichment scenario.

1.5 The Second Parameter Problem and the Case of NGC 2808

Based on the single-generation scenario and stellar evolution, globular clusters with the same age and metallicity would be expected to have very similar horizontal branches. There are examples, however, of clusters which have the same metallicity, indeed which by all standard measures are identical, yet

which have very different horizontal branch morphologies. An example of this would be M3 and M13 which are very similar in metallicity but have different HB luminosities relative to the main-sequence turnoff and show different HB morphologies (Rey et al., 2001). Other clusters simply exhibit peculiar internal HB morphologies such as the sloped horizontal branches of NGC 6388 and NGC 6441 (Sweigart & Catelan, 1998) or the bifurcated, extended horizontal branch of NGC 2808. These effects cannot be explained by overall cluster metallicity, a varying IMF or by differential reddening across the cluster. What is needed is an additional mechanism, a so-called second parameter, which can affect the horizontal branches of globular clusters but leave the rest of their stellar populations unchanged.

There are various possible second parameters of which the following list is not exhaustive. One possibility is that some clusters have enhanced helium. Since $X + Y + Z = 1$ where X is the hydrogen fraction and Y is the helium fraction it is possible for two clusters with the same Z value to have different X and Y values. This affects the metallicity with respect to hydrogen which, as mentioned in Section 1.3 affects the position of stars on the horizontal branch. A cluster with a higher helium content (one source of which could be self-enrichment) would be expected to have a bluer horizontal branch. Another possibility is rotating RGB stars. Rotation is known to delay the onset of helium ignition in the core and would lead to HB stars with anomalously high helium core masses, again affecting their position on the HB. Deep mixing in the envelopes of RGB and HB stars could also lead to different atmospheric chemistry which would in turn lead to differing effective temperatures and luminosities. Age is another factor that has been suggested. Cluster ages are

usually determined by looking at the location of the main-sequence turn-off (where main-sequence stars become RGB stars) in the CMD or by looking at the white-dwarf cooling sequence. These methods are rather model dependant meaning it is difficult to pin down cluster ages exactly. Thus globular clusters that appear coeval in one observation may actually differ significantly in age and their horizontal branches would be at a different stages of evolution. Indeed Rey et al. (2001) claim that this is the case with M3 and M13. Finally, dynamical interactions between the stars may play a role and indeed close encounters between stars may indeed trigger some of the processes just mentioned. It is well-known that several features of globular clusters, such as blue stragglers, appear mostly in dense stellar environments so a link between dynamics and stellar evolution is well-established. It is also possible that all these processes play a role in different clusters and that several may be active in the same cluster. This makes the second parameter problem rather delicate and it is important to distinguish between different physical processes which may produce the same observational effects.

In particular we consider NGC 2808, a globular cluster which exhibits a very peculiar horizontal branch morphology, possibly a result of a helium self-enrichment scenario. NGC 2808 is a southern galactic globular cluster first observed in detail in the late 1960s (Alcaino, 1969). It is quite massive at $1.6 \times 10^6 M_{\odot}$, has a moderately high velocity dispersion $\sigma_o = 13.4 km/s$ (Pryor & Meylan, 1993) and is relatively metal rich with $[Fe/H] = -1.09$ (Harris, 1996). As early as 1974 a peculiar morphology (both bimodal and extended) was discovered in the horizontal branch (HB) of the (CMD) of NGC 2808 (Harris, 1974) and is shown in Figure 1.2 (Bedin et al., 2000).

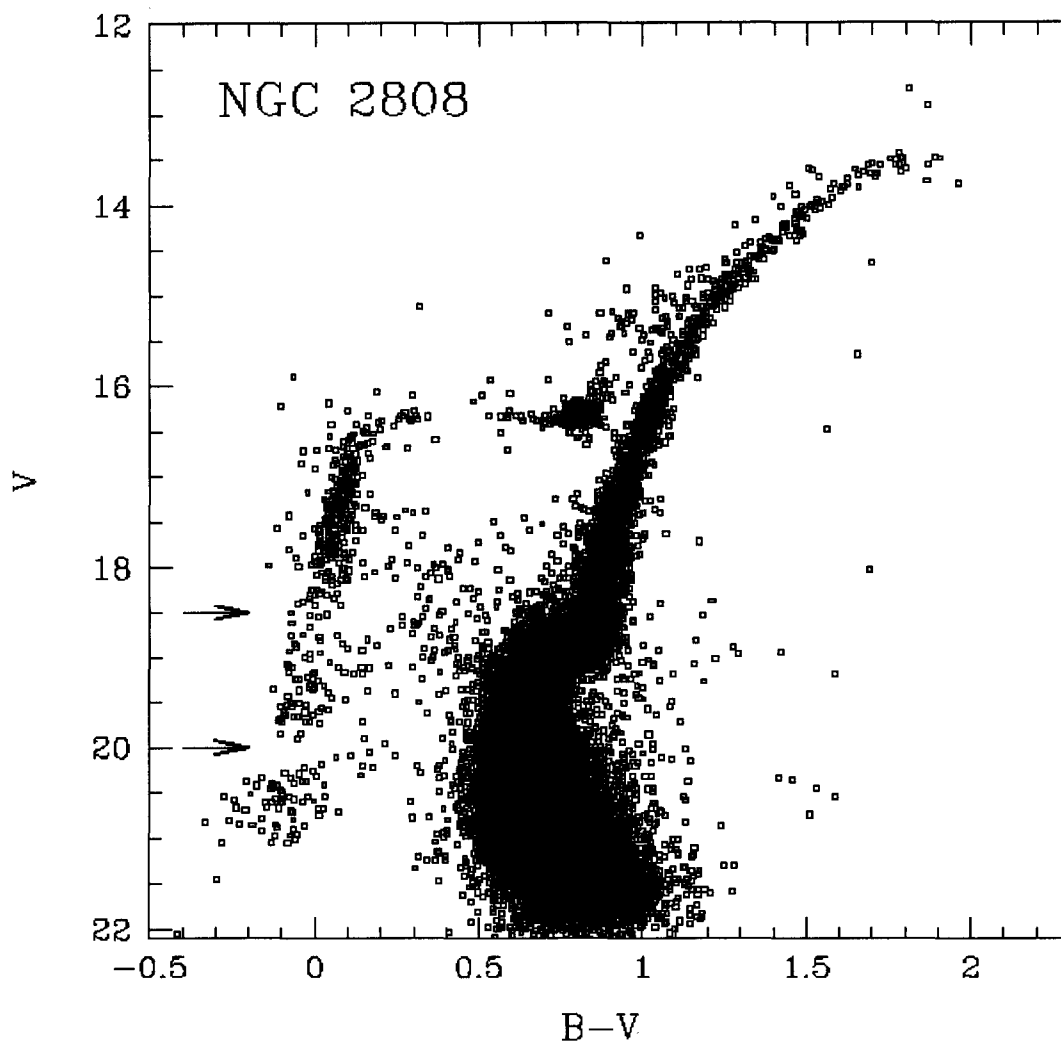


Figure 1.2 The horizontal branch of NGC 2808 is on the upper left-hand side of the diagram. It is distinctly bimodal with a red segment (RHB) at $(B - V) \sim 0.5$ and a very extended blue segment (BHB) centered on $(B - V) \sim 0$ and covering a magnitude range 16 – 21. The blue horizontal branch also shows a multimodal distribution of extended blue tails (top to bottom EBT 1, EBT 2 and EBT 3). This is very different from the canonical result shown in Figure 1.1 (Bedin et al., 2000).

The horizontal branch of NGC 2808 consists of both a small horizontal clump (hereafter called the red horizontal branch or RHB) and a long, extended tail reaching vertically from 16th to 22nd magnitude (hereafter called the blue horizontal branch or BHB). The BHB is also distinctly multi-modal with three distinct groups (called from top to bottom extended blue tails (EBTs) 1, 2 and 3). This is a very different morphology from the canonical morphology shown in Figure 1.1 and it is reminiscent of the second parameter problem but is different in detail. Specifically, most second parameter clusters do not display the distinct horizontal branch bifurcation and lack the RHB. Thus it becomes necessary to explore more complex scenarios, such as self-enrichment, to explain the horizontal branch of NGC 2808.

One explanation for the anomalous morphology of the HB of NGC 2808 is to assume that the BHB stars are helium enriched while the RHB stars contain the cosmological helium abundance of $Y \sim 0.24$ (D’Antona et al., 2002). It is possible that other anomalous CMD morphologies can be explained through helium enrichment as well. Notably the double main sequence of the massive cluster ω Centari can be explained if the blue main sequence stars are helium enriched (Piotto et al., 2005)* and indeed D’Antona et al. (2005) claim helium enrichment in some 20% of main sequence stars for NGC 2808 (although this case is less clear cut). The enrichment cannot be attributed to helium variations across the primordial cloud since the necessary levels of enrichment are extreme ($Y \sim 0.32 - 0.4$ is needed in EBT 3 (D’Antona & Caloi, 2004), (D’Antona et al., 2005)) and the helium must arise from stellar

* ω Centari has many other peculiarities and is thought to be the core of a stripped dwarf galaxy. It cannot be considered typical of galactic globular clusters

processes through self-enrichment. It has been argued (Gnedin et al., 2002) that the more massive globular clusters have sufficient self-gravity to retain the low-velocity ejecta from AGB stars (and in the case of the most massive even some of the ejecta from Type II supernova) and it is possible that NGC 2808 is one of these clusters (D’Antona & Caloi, 2004). This leads to a scenario in which helium self-enrichment from AGB stars produces the horizontal branch morphology of NGC 2808. In particular D’Antona & Caloi (2004) propose a model where NGC 2808 has experienced two stellar formation events. The first event features a top-heavy mass function that enhances the number of $3 - 5M_{\odot}$ stars. These evolve to the AGB phase in ≤ 200 Myr and, through the extensive mass loss previously discussed, enrich the interstellar medium (ISM) with helium (and other elements). A second generation of stars then forms from the helium-enriched ISM. Since there is expected to be a fairly wide range in ages on any horizontal branch a characteristic age difference of ≤ 200 Myr would not be observable (the overall age of NGC 2808 is about 12 Gyr) but the helium difference in the populations would be. The low-mass stars in the first generation would form the RHB of NGC 2808 and the enriched second generation would form the BHB. The multi-modality of the BHB (EBTs 1, 2 and 3) can be explained by varying levels of helium enrichment produced either by several minor stellar formation events producing different levels of helium enrichment or possibly by differential helium enrichment across the cluster. Modeling more than two generations or trying to account for differential spatial helium enhancement is beyond the scope of our project. Thus in this paper we do not try to model the origin of the substructure in the BHB.

1.6 Our Proposal

D'Antona and Caloi have shown through stellar evolution models that given certain assumptions sufficient helium can be produced to explain the BHB. If enhancements in other elements produced by AGB stars are ignored and the top-heavy mass function is accepted, the scenario may be plausible on the basis of stellar chemistry. The massive first generation may, however, have effects on both the dynamics and population of the cluster. Specifically the high mass of the initial generation and the effect of adding a second generation to a dynamically evolved object could have noticeable dynamical consequences. In particular we will be searching for any dynamical instabilities in the overall system produced by the introduction of the second generation. In addition the first generation will leave many intermediate-mass remnants, primarily white dwarfs, which should be observable (Hansen et al., 2002). We propose to use Starlab, an N-body code with a full suite of stellar evolution algorithms, to explore the dynamical evolution of a globular cluster in the D'Antona and Caloi two-generation formation scenario. We will use our models to investigate the plausibility of this scenario.

Bibliography

Alcaino, G. 1969, ApJ, 156, 853

Bedin, L. R., Piotto, G., Zoccali, M., Stetson, P. B., Saviane, I., Cassisi, S., & Bono, G. 2000, A&A, 363, 159

D’Antona, F., Bellazzini, M., Caloi, V., Pecci, F. F., Galleti, S., & Rood, R. T. 2005, ApJ, 631, 868

D’Antona, F. & Caloi, V. 2004, ApJ, 611, 871

D’Antona, F., Caloi, V., Montalbán, J., Ventura, P., & Gratton, R. 2002, A&A, 395, 69

de Boer, K. S. 1999, in ASP Conf. Ser. 167: Harmonizing Cosmic Distance Scales in a Post-HIPPARCOS Era, ed. D. Egret & A. Heck, 129–139

Gnedin, O. Y., Zhao, H., Pringle, J. E., Fall, S. M., Livio, M., & Meylan, G. 2002, ApJ, 568, L23

Hansen, B. M. S., Brewer, J., Fahlman, G. G., Gibson, B. K., Ibata, R., Limongi, M., Rich, R. M., Richer, H. B., Shara, M. M., & Stetson, P. B. 2002, ApJ, 574, L155

Harris, W. E. 1974, ApJ, 192, L161

—. 1996, AJ, 112, 1487

Kroupa, P. 2002, *Science*, 295, 82

Piotto, G., Villanova, S., Bedin, L. R., Gratton, R., Cassisi, S., Momany, Y.,
Recio-Blanco, A., Lucatello, S., Anderson, J., King, I. R., Pietrinferni, A.,
& Carraro, G. 2005, *ApJ*, 621, 777

Pryor, C. & Meylan, G. 1993, in *ASP Conf. Ser. 50: Structure and Dynamics
of Globular Clusters*, 357–371

Rey, S.-C., Yoon, S.-J., Lee, Y.-W., Chaboyer, B., & Sarajedini, A. 2001, *AJ*,
122, 3219

Sweigart, A. V. & Catelan, M. 1998, *ApJ*, 501, L63

Chapter 2

Stellar Dynamics

We outline the basics common to all N-body models, discuss some general issues and give a detailed description of what standard N-body simulations yield with a variety of physical effects included. Section 2.1 draws heavily from Heggie & Hut (2003) and most of the conclusions and comments are condensed from this source.

2.1 Basics of N-Body Modeling

N-body modeling involves tracking the evolution of a system consisting of N discrete particles each of which interacts with the others. In an astrophysical context each of the bodies normally represents a discrete mass and the interaction is gravitation. Astrophysical N-body modeling comes in two flavors: collisionless and collisional. The difference between the two is not necessarily direct collision of particles (although these can be included) but rather that in collisionless simulations two and three-body effects are not explicitly modeled whereas in collisional simulations they are. Collisionless N-body models are most valid in systems that are very large, that have long dynamical timescales

(such as galaxies) or where the particles are naturally smoothed and softened (such as dark matter). Such conditions routinely exist in the context of galaxies and cosmology, and cosmological N-body codes are generally collisionless. Collisional N-body modeling is relevant to the field of star cluster dynamics and modeling systems where each particle represents a single star. Globular clusters are dense stellar environments with $N \sim 10^6$, a dynamical timescale less than a Hubble time and where two-body relaxation effects are important. This makes them manifestly collisional systems and methods that take into account few-body interactions (particularly binary systems and two- and three-body scattering events) are necessary for an accurate treatment.

Although collisional, much progress has been made in the study of globular cluster dynamics with the use of collisionless methods. The computational power required for collisional modeling with realistic numbers of particles has not been available until recently and out of necessity early stellar dynamicists employed collisionless methods with varying degrees of success. Two of these methods, thermo-statistics and the Fokker-Planck equation are representative of their efforts and deserve some attention before collisional N-body simulations are discussed.

2.1.1 Thermo-statistics

Globular clusters have $O(10^6)$ particles and as such it seems that classical methods in statistical physics, such as canonical ensembles employed in plasma physics where inverse-square laws are common, might be applicable. There are three related problems with this approach. The first is that it is

possible to speak of a neutral, uniform, infinite distribution of plasma in equilibrium. Since gravity is both long-range and exclusively attractive, no such equilibrium is possible for a gravitational system and standard statistical formulations in plasma physics cannot be applied. The second problem is that due to the presence of positive and negative charges in a plasma there is a screening length (called the Debye length) within which many effects can be localized and which provides a natural decoupling of scales. Again due to the long-range and attractive nature of gravity, no such length exists in gravitational systems and there is no decoupling of scales. Finally if a volume containing a uniform density of stars is enlarged while the density and temperature are kept constant the kinetic energy scales as $T \propto M$ but the potential energy scales as $U \propto M^{5/3}$. Thus in gravitational N-body systems energy is not extensive but superextensive and conventional thermo-statistics do not apply. Despite its limited applicability interesting early results on N-body gravitational dynamics, particularly the theory of gravothermal instability (Antonov, 1962), were produced using a statistical approach. Briefly, gravothermal instability is a product of the fact that gravitationally dominated systems have a negative heat capacity and heat up when energy is removed from them. It can be shown (Binney & Tremaine, 1987) that an isothermal gravitational sphere in contact with a heat bath (such as the core of a star cluster in contact with its halo) is unstable and will collapse on a timescale governed by its thermal diffusion timescale (in star clusters this is the two-body relaxation timescale). This is sometimes called the gravothermal catastrophe. Core collapse of stellar clusters after 10-15 initial half-mass relaxation times has indeed be confirmed

in direct N-body simulations (Makino, 1996) and gravothermal instability is still a very important concept in stellar dynamics.

2.1.2 Fokker-Planck Methods

The Fokker-Planck equation is a phase-space statistical treatment of stellar dynamics (Heggie & Hut, 2003) and is essentially the weak-scattering limit of direct N-body integration. In the Fokker-Planck model stars are given probability distribution in phase space, f , which is usually normalized such that $N = \int f d^3\mathbf{r} d^3\mathbf{v}$. This distribution is then inserted into the collisionless Boltzmann equation:

$$\frac{\partial f}{\partial t} + \mathbf{v} \cdot \nabla_{\mathbf{r}} f - \nabla \phi \cdot \nabla_{\mathbf{v}} f = 0$$

where ϕ is the potential. It is possible to modify this equation to approximate two-body relaxation effects, resulting in either the Boltzmann equation or the Fokker-Planck equation. The latter is most commonly used in stellar dynamics and for the case of an a spherical system in a state of quasi-dynamic equilibrium with an isotropic distribution of velocity takes the form:

$$\frac{\partial f}{\partial t} \frac{\partial s}{\partial E} - \frac{\partial f}{\partial E} \frac{\partial s}{\partial t} = \frac{\partial}{\partial E} (D_E f) + \frac{1}{2} \frac{\partial^2}{\partial E^2} (D_{EE} f)$$

where D_E and D_{EE} are diffusion coefficients in the first and second derivative of energy representing the effect of close encounters, and s is the volume in phase space inside the hypersurface with energy E . This equation can then be solved numerically, normally using Monte Carlo simulations or finite difference methods. The Fokker-Planck method, while not truly collisional, is considered to be the most accurate method for dealing with dense stellar systems short of

direct N-body intergration and is much more computationally tractable. The method has had good success in matching observations of globular clusters (e.g. Drukier (1995)). It has been shown (e.g. Drukier et al. (1999) and Preto et al. (2004)) that results from Fokker-Planck and direct N-body simulations are generally consistent so results from Fokker-Planck models are useful for comparison with direct N-body simulations. Fokker-Planck is, however, still a collisionless approximation to a collisional system and this approximation is not accurate in all situations (see Spurzem & Takahashi (1995) and Portegies Zwart et al. (1998) for some discussion of regions where the Fokker-Planck approximation is invalid). For this reason stellar dynamicists are turning to direct N-body simulations.

2.1.3 Direct N-body Simulations

Direct N-body simulations involve the explicit integration of the Newtonian equations of motion for an N-body gravitational system (Heggie & Hut, 2003):

$$\frac{\partial^2 \mathbf{r}_i}{\partial t^2} = -G \sum_{j=1, j \neq i}^{j=N} m_j \frac{\mathbf{r}_i - \mathbf{r}_j}{|\mathbf{r}_i - \mathbf{r}_j|^3}$$

This is probably the most intuitively obvious way of approaching collisional stellar dynamics and it is, in principle, the most accurate. Since no problem beyond the two-body problem can be solved analytically, however, a numerical solution is necessary and the computational power required is immense. This is related both to the large range of length and time scales that must be resolved in collisional N-body modeling and the high-degree of accuracy required in stellar-dynamical simulations. The size of a typical cluster is some

14 orders of magnitude larger than the size of a neutron star (its smallest typical member) and the disparity between dynamical time scale for a globular cluster (on the order of a Hubble time) and the time scale for the two- and three-body scattering interactions which are important to the evolution of collisional systems can be even larger. The CPU cost for collisional direct N-body simulations also inherently scales as N^3 which has made large simulations difficult. Simulations of collisional N-body systems also require a higher degree of accuracy than do collisionless (particularly cosmological) simulations (Hut & Makino, 1999). This, combined with the fact that collisional N-body simulations generally require many more timesteps relative to their collisionless counterparts means that simulations of star clusters have been limited to order 10^4 particles while cosmological simulations are easily able to include 10^6 (and even up to 10^9) particles. General-purpose supercomputers have been of less help in advancing collisional N-body simulations than collisionless ones. This is partly because tree codes and other approximation schemes destroy the required degree of accuracy in collisional simulations (Barnes & Hut, 1986) and discrete summing mechanisms must be used. There is also a communications bottleneck in a parallel situation since each particle explicitly requires information from each other particle in order to advance the simulation. Schemes where parallelization is used to advance many particles simultaneously in a block timestep can be used but in most N-body simulations particles are allowed to have an individual timestep in order to decouple the few particles with a short timescale from the longer timescale of the system. As such care must be taken in implementing block timesteps in order to neither reduce the timestep of the entire system to that of the shortest particle

nor to advance some particles with a timestep that is too long and reduce the accuracy of the simulation. The best results for collisional N-body modeling have come via special-purpose hardware devices such as the GRAPE series of gravitational N-body accelerators (see Section 3.2). By the combination of special-purpose hardware and individual time-stepping codes it is now possible to perform simulations of order 10^4 particles in a reasonable timescale (multiple simulations over the length of an M.Sc. program for instance). Although this is still an order of magnitude less than the number of stars in a standard globular cluster, the accuracy and explicit treatment of few-body encounters possible in direct N-body simulations have made them the preferred approach for studying collisional stellar systems. This is the approach we choose for our project.

2.2 Explicit Behavior of N-body Systems

It is important to understand how simple N-body systems evolve and how this varies with the inclusion of various physical processes such as an initial mass functions and mass-loss due to stellar evolution. It is also useful to understand some of the specialized units and diagnostics that appear in stellar dynamics and to consider the initial conditions that can be chosen for an N-body problem.

2.2.1 Scales and Diagnostics

In order to facilitate comparison between simulations and observation it must be possible to express stellar dynamical problems in terms of units used normally in astrophysics: distance in parsecs, time in Megayears and velocities in kilometers per second. In practice these units are not convenient units in which to actually perform or compare simulations on a dynamical basis and there are a widely (although not universally) used set of units called virial, or Heggie units (Heggie & Mathieu, 1986) that are more useful. In Heggie units the system is assumed to start in virial equilibrium (the kinetic energy is exactly twice the potential energy $2K + W = 0$). The gravitational constant G is chosen to be unity and the length and mass are scaled such that the total mass $M = 1$ and the total energy $E = -\frac{1}{4}$. This makes the virial radius $\left(R_v = -\frac{GM^2}{4E}\right)$ the length unit and the time unit becomes $T = \frac{R_v^{3/2}}{\sqrt{GM}}$. This system is often used for numerical computations and also for comparison between N-body simulations. Given physical values for the gravitational constant, total mass and either length or time they can be scaled back to physical units again.

Another commonly used time scale is the relaxation time for the star system. This is the number of system crossing times necessary for the velocity of a given star to become the same as if it were moving across a smooth potential (essentially the timescale over which two-body effects cease to be important). There are several order of magnitude estimates for the relaxation time and the relaxation time at the half-mass radius (called the half-mass relaxation time) defined by Spitzer (1987) as $T_{RH} = \left(\frac{R_{HM}^3}{GM}\right)^{1/2} \frac{N}{8 \log \Lambda}$ is used in this paper. The

half-mass radius R_{HM} is the radius of an imaginary sphere containing half the mass of the system and Λ is called the Coulomb logarithm which, following Giersz & Heggie (1994), we take to be $0.1N$. Systems that have evolved for the same number of relaxation times should be in the same stage of dynamical evolution regardless of their physical parameters so this time unit is useful for comparing N-body simulations to each other. It is important to note that the half-mass relaxation time is a dynamically evolving quantity and that in general it is initial half-mass relaxation times that are reported.

One diagnostic tool that will be seen in any analysis of N-body simulations are the Lagrangian radii. They are the primary method for exploring the spatial behavior of N-body systems and as such they deserve special mention. The $x\%$ Lagrangian radius is the radius of an imaginary sphere placed at the center of an N-body system containing $x\%$ of the total mass of the system. In particular R_{HM} corresponds to the 50% Lagrangian radius. The Lagrangian radii have characteristic behaviour depending on the initial conditions and the physics included in a simulation as will be seen in the following sections.

2.2.2 Initial Conditions

An adjustable parameter in N-body simulations is the starting configuration of the stars in phase space. Although it can be shown that there is no stable equilibrium to which a gravitational N-body system will evolve (Heggie & Hut, 2003) it is common to start out with the system in an equilibrium configuration and allow it to evolve from there. Two popular equilibrium models are the Plummer model and the King model.

The Plummer model (Plummer, 1911) is an $n = 5$ polytrope where $f = \frac{3.2^{7/2}}{7\pi^3} \frac{a^2}{G^5 M^4 m} (-E)^{7/2}$, the mass density is given by $\rho = \frac{3M}{4\pi a^3} (1 + \frac{r^2}{a^2})^{-5/2}$ and the potential is $\phi = -\frac{GM}{\sqrt{a^2+r^2}}$. M , the total mass of the system, and a , the characteristics scale radius, are the free parameters. The Plummer model is analytic and due to its venerability it is very well studied making it a popular choice for purely numerical studies. The King model (King, 1966) is designed to fit observations of current (dynamically evolved) globular clusters and is formed by taking a lowered Maxwellian potential $f = f_0(e^{-2j^2E} - e^{-2j^2E_0})$ for $E < E_0$ and $f = 0$ for $E \geq E_0$ where E_0 is the escape velocity and j is a constant related to the one-dimensional initial velocity dispersion ($\sigma^2 = \frac{1}{2j^2}$). The King model is specified by σ , the initial central density ρ_0 , and a dimensionless potential $W_0 = 2j^2(E_0 - E_c)$ where E_c is the energy of a star at rest at the center. The King model may be a better representation of current globular clusters, but we follow Hurley et al. (2005) in choosing Plummer initial conditions. Because of its venerability there are many simulations initiated with Plummer models available in the literature for comparison with our simulations. Because the King model was designed to fit current conditions it is also not obvious that it is an appropriate choice for an initial distribution. It has also been shown (Hurley & Shara, 2003) that a Plummer model will evolve fairly rapidly into something resembling a King model through natural dynamical processes. For these reasons we consider our choice of a Plummer model to be appropriate for our project.

Since stars form with a spectrum of masses it is necessary to replicate this in simulations. This is done through choosing an appropriate initial mass function (IMF). There is thought to be a universal IMF for all globular clusters

although there are currently several mass functions in common use (Kroupa, 2002). One of the most standard is the Salpeter IMF (Salpeter, 1955) which is a power law IMF of the form $\frac{dN}{dM} \propto M^{-2.35}$. This mass function is thought to represent the inferred IMF of globular clusters (Kroupa, 2002) fairly well. It is also a standard IMF to use for any non-specific work in globular cluster dynamics (meaning most available comparisons use this IMF). This is the IMF we choose as our baseline for testing the top-heavy IMF prescribed by D’Antona & Caloi (2004) and discussed in more detail in Chapter 3.

2.2.3 The Case of Equal Masses

The simplest N-body system is the one where all of the particles have the same mass. This model contains little physics and is thus an ideal case for studying pure N-body dynamics. In part of their series on the statistics of N-body simulations Giersz & Heggie (1994) carefully constrain the behavior of equal-mass N-body systems by statistically comparing the results of 220 simulations starting from Plummer models and with varying numbers of particles. The overall result is shown in Figure 2.1.

The general behavior is that the 50% Lagrangian radius (the half-mass radius) remains flat while the outer radii expand and the inner radii contract. The contraction will continue until the stellar density at the center of the cluster approaches infinity, a phenomenon called core collapse. The time to core collapse for a globular cluster is another important dynamical timescale and cluster evolution is usually divided into its pre- and post-core collapse phase. After post-core collapse the cluster core undergoes several expansions

and contractions (known as gravothermal oscillations) and the cluster dissipates away. It is demonstrated in Figure 2.1 that the effect of larger N is to increase the time to core collapse which is consistent with the assumption the the evolution of the cluster is driven by two-body relaxation. We have computed a similar model using a Plummer model with $N = 8192$. Figure 2.2 demonstrates that our results are consistent with the findings of Giersz & Heggie (1994). We cannot expect exact quantitative agreement since the results of Giersz & Heggie (1994) are an average over 220 simulations and ours is a single realization.

2.2.4 Initial Mass Functions

The next step to be taken is to allow the stars to have a spectrum of masses as defined by an initial mass function. In another paper in the series on statistics of N -body simulations Giersz & Heggie (1996) present the consequences of including a mass function in the simulations. They compare 152 simulations ranging from $N = 250$ to $N = 500$ using Plummer initial conditions and a Salpeter IMF. The primary result is the appearance of a phenomenon known as mass segregation where the more massive stars migrate to the center of the cluster and the less massive stars are ejected to the outskirts. This phenomenon is driven by two-body relaxation and is a consequence of the cluster trying to achieve equipartition of energy throughout phase space. Mass segregation is illustrated by Figure 2.3 which shows that the average mass contained within a Lagrangian radius decreases with increasing distance from the center. It is also possible to track mass segregation by plotting Lagrangian radii for

the massive stars separately from the Lagrangian radii of the entire system and seeing if the distribution is different.

We have performed a similar simulation with $N = 8192$ particles the results of which are shown in Figure 2.4. We find results that are qualitatively consistent with Giersz & Heggie (1996). Quantitative agreement is again not expected since Figure 2.3 is based on an average of multiple simulations.

2.2.5 Stellar Evolution

As stars evolve, they lose mass, experience radius variations, change in luminosity etc. From the standpoint of dynamics it is the mass loss that is important (although radius variations can be important in binary systems and the pre-main sequence phase) because it affects the gravitational dynamics of individual stars and also reduces the potential well of the system. Fukushige & Heggie (1995) investigate the effect stellar evolution on the evolution of a globular cluster with the results shown in Figure 2.5.

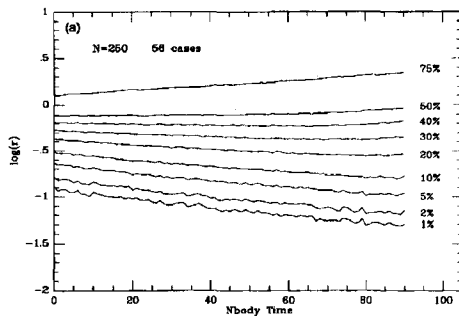
The primary effect of mass-loss is to cause the clusters to dissipate much more quickly than they would otherwise (indeed sometimes before core collapse). This is not surprising since the loss of mass continuously reduces the potential of the bound system. It is also worth noting that simulations with a flatter initial mass function (i.e. the one with the most high-mass stars) dissipates much more quickly than the ones with steeper mass functions and fewer high mass stars. This result is confirmed through Monte-Carlo simulations by Giersz (2001) and Joshi et al. (2001). This is not surprising since high-mass stars lose a much greater fraction of their mass at a lower age than do low

mass stars. Fukushige & Heggie (1995) also compare total mass as a function of time for varying numbers of particles as shown in Figure 2.6.

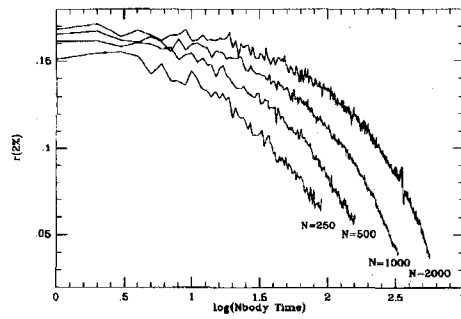
Due to two-body relaxation effects contributing to cluster evaporation the mass-loss rate of the cluster is somewhat dependent on the number of particles used in the realization. The mass-loss is very weakly dependent on the total number of stars in the flat mass function case and becomes more strongly dependant in the case of the intermediate and steep mass functions. In all cases the difference between $N = 8192$ and $N = 16384$ is less significant than the difference between $N = 8192$ and any lower number, indicating that if $N \geq 8192$ is chosen then problems due to small-number statistics can be avoided (although more particles are always better given sufficient time). We have computed an $N = 8192$ model starting with a Salpeter mass function including stellar evolution the results of which we present in Figure 2.7.

This corresponds to case (b) from Figure 2.5. Fukushige & Heggie (1995) include a tidal stripping radius, providing a means of removing stars from the simulation and causing their cluster to evaporate more quickly than ours. Modulo the tidal stripping our results are consistent.

Now that we have confirmed that our baseline simulations are in agreement with the literature, we can proceed to address the problem in which we are truly interested: the behaviour of an N-body system with a top-heavy IMF and a second generation.



(a) Lagrangian Radii



(b) Number Dependence

Figure 2.1 On the left is shown the evolution of the Lagrangian radii for a cluster of equal mass particles. On the right is shown the variation of the 2% Lagrangian radius for different numbers of particles in the simulation (Giersz & Heggie, 1994).

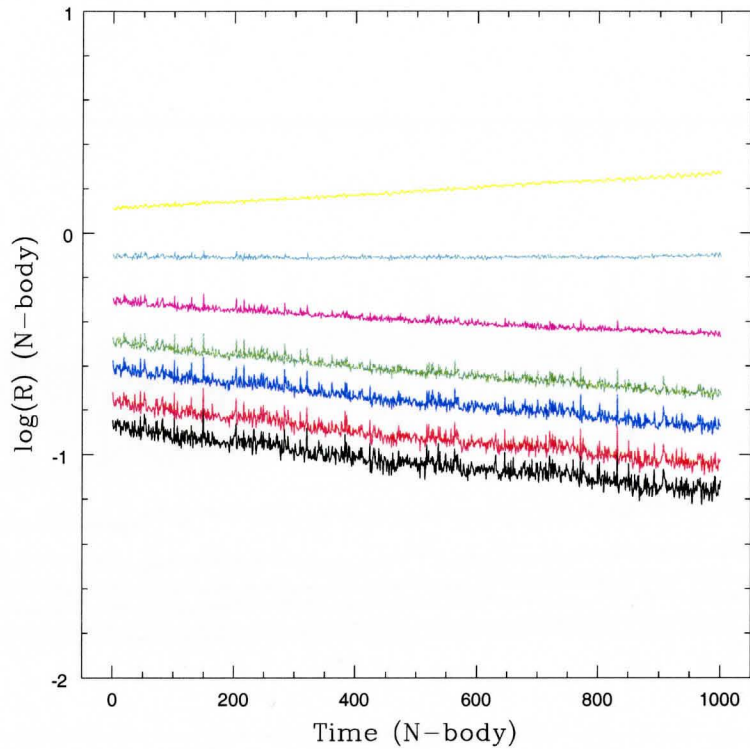


Figure 2.2 Representative Lagrangian radii from an $N = 8192$ particle simulation. From bottom to top the 1%, 2%, 5%, 10%, 25%, 50% and 75% Lagrangian radii. Due to the larger number of particles the relaxation time of our simulation is much longer than in Giersz & Heggie (1994). Thus the end of our simulation corresponds to approximately timestep 50 in Figure 2.1 (a).

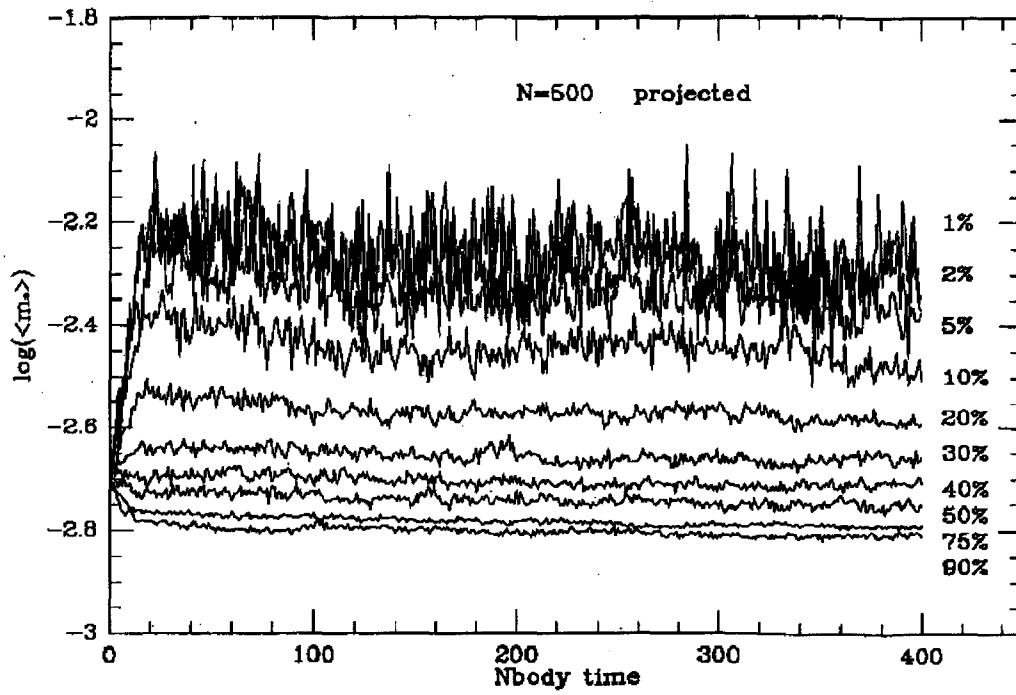


Figure 2.3 The average mass contained within each Lagrangian radius in the case of a Salpeter mass function (Giersz & Heggie, 1996).

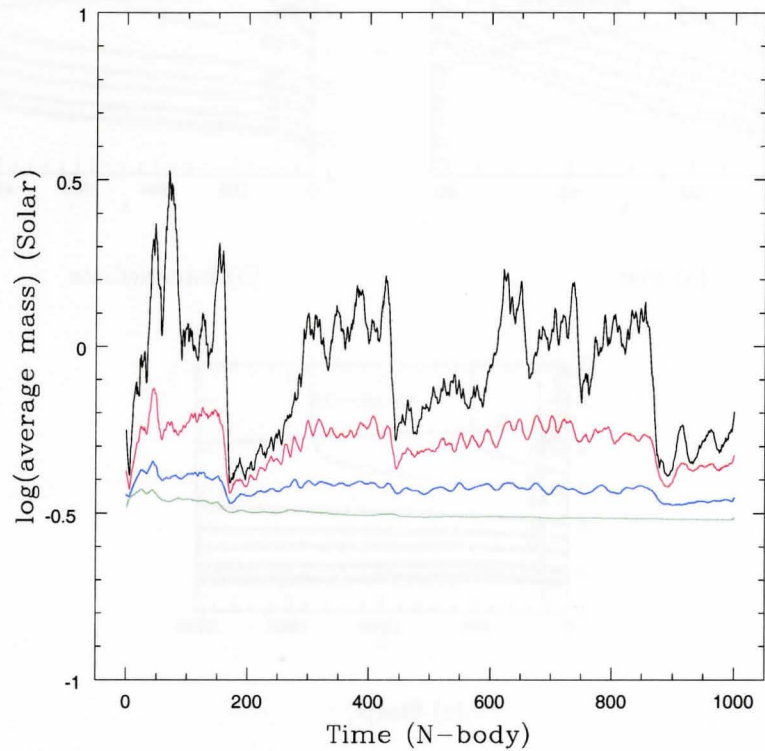
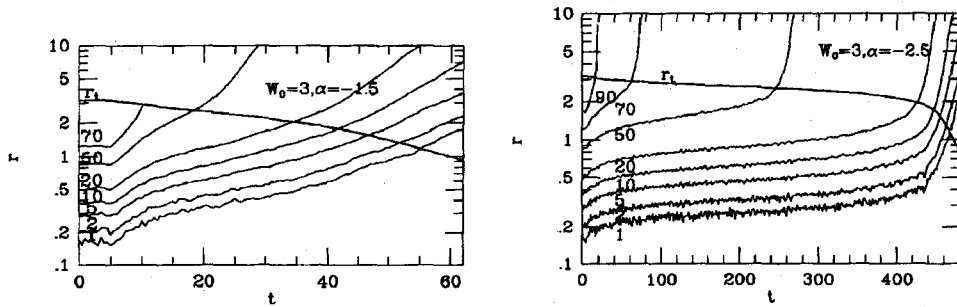
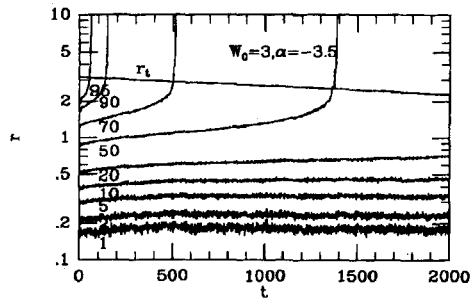


Figure 2.4 The average mass contained within each Lagrangian radius in the case of a Salpeter mass function. Black is 10% red is 25%, blue is 50% and green is 75%. Due to the larger number of particles in our simulation the relaxation time is much longer than in the Giersz & Heggie (1996) case and the end of our simulation corresponds to timestep 100 in Figure 2.3.



(a) Flat

(b) Intermediate



(c) Steep

Figure 2.5 The effect of stellar mass-loss on the evolution of the Lagrangian radii. In each case α is the slope of the IMF and W_0 is the King model concentration parameter (not very concentrated in this case). r_t is the tidal stripping radius of the cluster. Simulation (a) corresponds to a top-heavy IMF such as prescribed in D’Antona & Caloi (2004), (b) corresponds closely to a Salpeter IMF and (c) would be an IMF with very few high-mass stars. We do not consider IMF’s of the (c) form in this paper but the result is included for completeness. (Fukushige & Heggie, 1995).

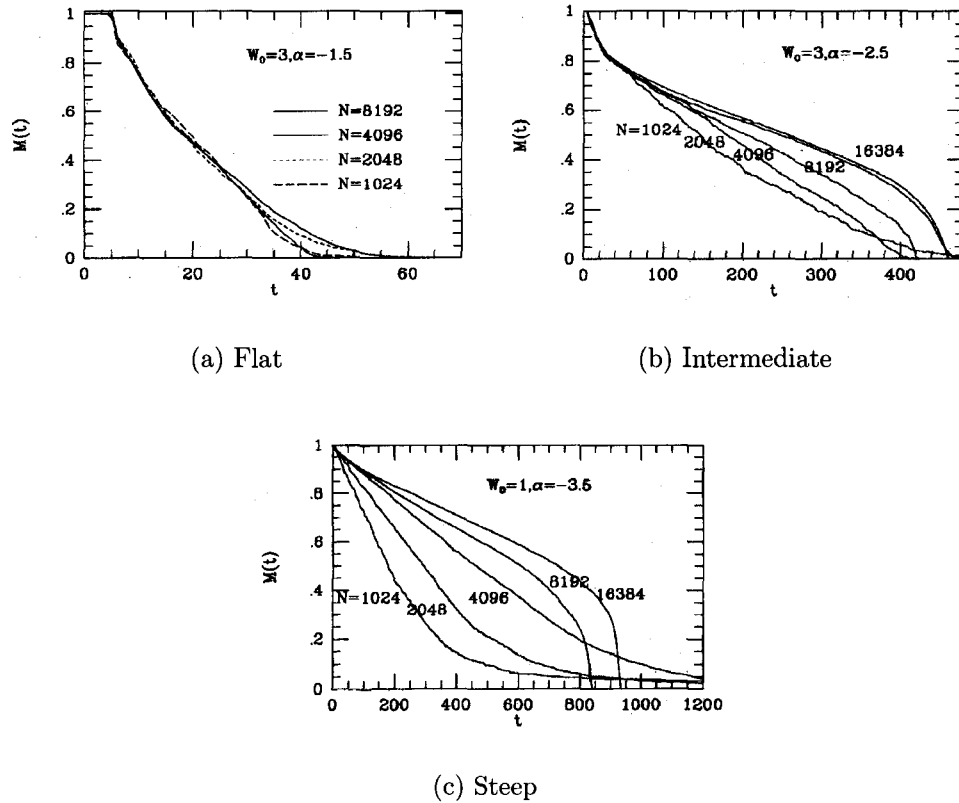


Figure 2.6 The number dependence of mass-loss due to stellar evolution. In cases (a) and (b) (the ones of interest in this paper) there is no significant number-dependence in the 8192-16384 particle regime. (Fukushige & HEGGIE, 1995).

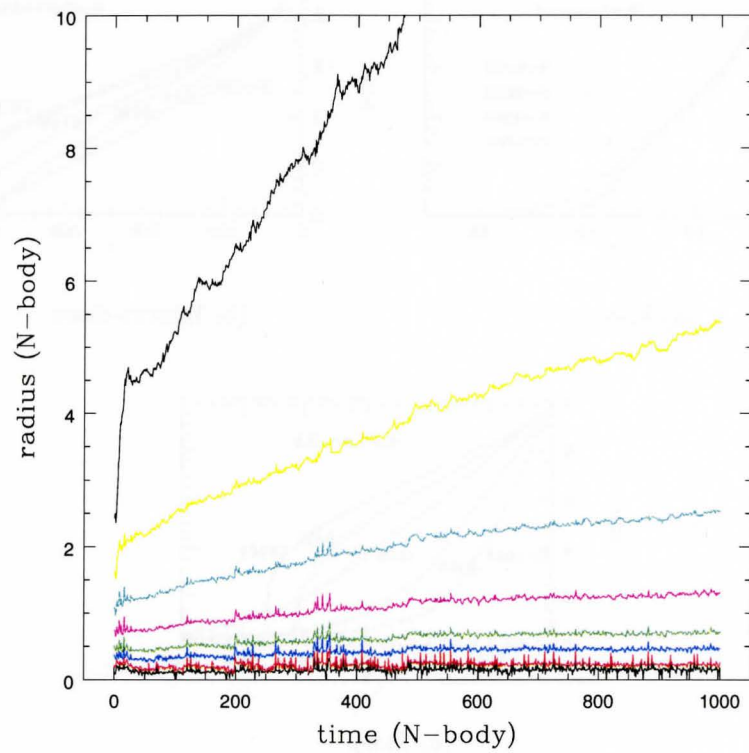


Figure 2.7 The evolution of the Lagrangian radii with mass loss. From top to bottom: 1%, 2%, 5% 10%, 25%, 50%, 75% and 90% Lagrangian radii. In this case our timestep is comparable to that in Figure 2.5.

Bibliography

- Antonov, V. A. 1962, Solution of the problem of stability of stellar system
Emden's density law and the spherical distribution of velocities (Vestnik
Leningradskogo Universiteta, Leningrad: University, 1962)
- Barnes, J. & Hut, P. 1986, *Nature*, 324, 446
- Binney, J. & Tremaine, S. 1987, *Galactic dynamics* (Princeton, NJ, Princeton
University Press, 1987, 747 p.)
- D'Antona, F. & Caloi, V. 2004, *ApJ*, 611, 871
- Drukier, G. A. 1995, *ApJS*, 100, 347
- Drukier, G. A., Cohn, H. N., Lugger, P. M., & Yong, H. 1999, *ApJ*, 518, 233
- Fukushige, T. & Heggie, D. C. 1995, *MNRAS*, 276, 206
- Giersz, M. 2001, *MNRAS*, 324, 218
- Giersz, M. & Heggie, D. C. 1994, *MNRAS*, 268, 257
- . 1996, *MNRAS*, 279, 1037
- Heggie, D. & Hut, P. 2003, *The Gravitational Million-Body Problem: A Multi-
disciplinary Approach to Star Cluster Dynamics* (The Gravitational Million-
Body Problem: A Multidisciplinary Approach to Star Cluster Dynamics, by
Douglas Heggie and Piet Hut. Cambridge University Press, 2003, 372 pp.)

- Heggie, D. C. & Mathieu, R. D. 1986, LNP Vol. 267: The Use of Supercomputers in Stellar Dynamics, 267, 233
- Hurley, J. R., Pols, O. R., Aarseth, S. J., & Tout, C. A. 2005, MNRAS, 363, 293
- Hurley, J. R. & Shara, M. M. 2003, ApJ, 589, 179
- Hut, P. & Makino, J. 1999, Science, 283, 501
- Joshi, K. J., Nave, C. P., & Rasio, F. A. 2001, ApJ, 550, 691
- King, I. R. 1966, AJ, 71, 64
- Kroupa, P. 2002, Science, 295, 82
- Makino, J. 1996, ApJ, 471, 796
- Plummer, H. C. 1911, MNRAS, 71, 460
- Portegies Zwart, S. F., Hut, P., Makino, J., & McMillan, S. L. W. 1998, A&A, 337, 363
- Preto, M., Merritt, D., & Spurzem, R. 2004, ApJ, 613, L109
- Salpeter, E. E. 1955, ApJ, 121, 161
- Spitzer, L. 1987, Dynamical evolution of globular clusters (Princeton, NJ, Princeton University Press, 1987, 191 p.)
- Spurzem, R. & Takahashi, K. 1995, MNRAS, 272, 772

Chapter 3

Numerical Tools

In this chapter the N-body code, Starlab, and the GRAPE-6 N-body accelerator used in this project are introduced. The modifications made to the basic distribution of Starlab are also discussed.

3.1 STARLAB

Starlab is a direct N-body integrator with a full suite of stellar and binary evolution algorithms. Its primary contributors have been Piet Hut, Steve McMillan, Junichiro Makino and Simon Portegies Zwart. Starlab and such information as is available for it can be found at <http://www.ids.ias.edu/~starlab/>.

Starlab is organized according to a tree structure although this does not reflect how forces are calculated (all forces between particles are calculated directly). Rather there is one root node with all single stars and binary systems considered daughter nodes of the root node and sisters to each other. Individual stars in binary systems are daughters of the binary node, not the root node. Since direct N-body force calculations are performed only between sister nodes, binary systems are treated as single particles when N-body evolu-

tion is performed on the entire system. This allows binary systems themselves to be evolved separately from the overall system and thus decouples binary from N-body evolution. This in turn decouples the short timescale of binary evolution from the much longer dynamical timescale of the N-body system and makes the code more efficient. An example of how this works in practice is found in Figure 3.1.

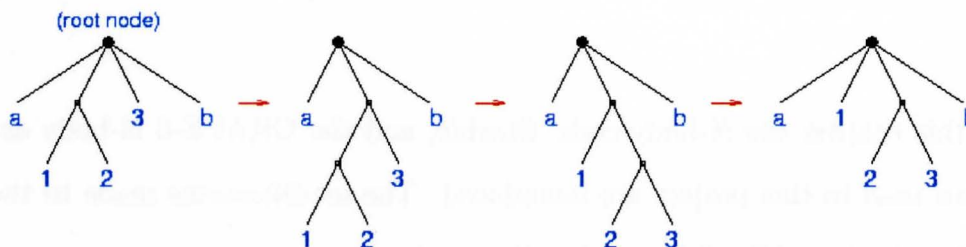


Figure 3.1 The tree structure of starlab in a three-body encounter. On the left is a system with four nodes, one of which is a binary. In the middle two there are three daughter nodes of the root one of which has two daughter nodes one of which is a binary. On the far right there are four nodes again one of which is a binary but the binary membership has switched due to the three-body encounter. From <http://www.ids.ias.edu/~starlab/kira/>

Reflecting this tree structure, Starlab is broken into two major components: the N-body integrator Kira, and SeBa, the routine that computes binary and stellar evolution.

3.1.1 Kira

Kira is the N-body integrator and is the largest single routine in Starlab. Its basic purpose is to step the entire system forward in time and to output logfiles of overall system information and snapshots of the properties of individual stars at specified intervals. As mentioned in Section 2.1.3, a high degree of accuracy

is needed in order for collisional N-body simulations to be reliable (this is particularly true in the post core collapse phase). Makino (1991) demonstrates that in order to reliably advance a direct N-body star cluster simulation to the postcollapse phase the energy error per crossing time should be of order no greater than 10^{-9} for which an integration scheme accurate to fourth-order is sufficient. Makino & Aarseth (1992) show that for the GRAPE architecture a Hermite integration scheme is the most efficient. With this in mind Starlab uses a fourth-order Hermite predictor-corrector scheme (Portegies Zwart et al., 2001) with block timestepping (McMillan, 1986). During a timestep δt the position vectors, \mathbf{x} , and velocity vectors, \mathbf{v} , for the particles are predicted using the acceleration, \mathbf{a} , and the second derivative of acceleration, called the jerk, \mathbf{j} , according to the prescription:

$$\begin{aligned}\mathbf{x}_p &= \mathbf{x} + \mathbf{v}\delta t + \frac{1}{2}\mathbf{a}\delta t^2 + \frac{1}{6}\mathbf{j}\delta t^3 \\ \mathbf{v}_p &= \mathbf{v} + \mathbf{a}\delta t + \frac{1}{2}\mathbf{j}\delta t^2\end{aligned}$$

where p stands for the predicted quantity. The predicted acceleration and jerk, \mathbf{a}_p and \mathbf{j}_p , are then calculated from the predicted position and velocity using standard Newtonian gravitational formulae. \mathbf{a}_p and \mathbf{j}_p are then used to define two correction factors:

$$\begin{aligned}\mathbf{k} &\equiv \frac{1}{2}\mathbf{a}''\delta t^2 = 2(\mathbf{a} - \mathbf{a}_p) + \delta t(\mathbf{j} - \mathbf{j}_p) \\ \mathbf{l} &\equiv \frac{1}{6}\mathbf{a}''' \delta t^3 = -3(\mathbf{a} - \mathbf{a}_p) - \delta t(2\mathbf{f} + \mathbf{j}_p)\end{aligned}$$

These are then used to correct the predicted position and velocity to give the final position and velocity reported by Starlab:

$$\mathbf{x}_c = \mathbf{x}_p + \left(\frac{1}{20}\mathbf{l} + \frac{1}{12}\mathbf{k} \right) \delta t^2$$

$$\mathbf{v}_c = \mathbf{v}_p + \left(\frac{1}{4}\mathbf{1} + \frac{1}{3}\mathbf{k} \right) \delta t$$

In a simple integration timestep the following actions are performed in the given order:

- (i) Determine which stars are to be updated next.
- (ii) Check for:
 - (a) Termination of run;
 - (b) Escaper removal;
 - (c) System re-initialization;
 - (d) Logfile output if specified (system properties);
 - (e) Snapshot output if specified (individual stellar properties).
- (iii) Perform low-order prediction of particle positions and velocities at the new time.
- (iv) Recompute acceleration and jerk at new position and velocity and correct position and velocity to fourth order.
- (v) Check for and initiate unperturbed motion (binaries).
- (vi) Check for collisions and mergers.
- (vii) Check for reorganization of tree (e.g. formation or dissociation of binaries removing or adding nodes at different levels).
- (viii) Check for and apply stellar and binary evolution.

It is also possible to include a galactic tidal field and tidal stripping of the cluster in kira but since we are only considering clusters in isolation in this paper these functions will not be examined.

3.1.2 SeBa

SeBa (whimsically named for the ancient Egyptian word ‘to teach’ or ‘the door to knowledge’ or ‘multiple star’ depending on the translation) is the subroutine of Starlab that deals with stellar and binary evolution

3.1.2.1 Stellar Evolution

The stellar evolution routine is based upon the semi-analytic time-dependant mass-radius relations outlined in Eggleton et al. (1989) (with corrections by Eggleton et al. (1990) and Tout et al. (1997)). These give the radius of a star as a function of time and initial mass on the zero-age main sequence (ZAMS). This prescription makes no distinct prediction for the mass of a stellar core and does not include mass-loss due to stellar winds. Both of these quantities are important for binary evolution and are thus accounted for according to an additional prescription of Portegies Zwart & Verbunt (1996).

Stars are divided by SeBa into several types depending on their mass, radius and age. Following are the types important to this project:

Main Sequence A star with core hydrogen burning.

Hertzsprung Gap A star in the rapid phase of evolution from the termination of the main sequence to the point where the hydrogen-depleted core collapses.

Subgiant Hydrogen shell burning RGB star.

Horizontal Branch Helium core burning star.

Supergiant Double shell burning star (AGB stars are in this category).

White Dwarf An electron-degenerate stellar remnant with a low- to

intermediate-mass progenitor. Subdivided into helium dwarf, carbon dwarf and oxygen dwarf based on composition.

Disintegrated Result of carbon detonation and a Type Ia supernova.

Neutron Star A neutron-degenerate stellar remnant with a high-mass progenitor. Subdivided into radio pulsar, X-ray pulsar and inert neutron star ($M < 2M_{\odot}$).

Black Hole Gravitationally collapsed stellar remnant with a high-mass progenitor. In Starlab a star with radius less than the event horizon.

There are also pre-main sequence stellar evolution routines available for SeBa (Wiersma et al., 2006) but since we are initiating our clusters from the ZAMS we do not use these in our project. Ultimately we need stellar evolution that will account for the mass-loss in the initial generation of stars and will predict the fraction of compact remnants it will leave. The basic distribution of SeBa is capable of doing this and no modification on our part is necessary.

3.1.2.2 Binary Evolution

As mentioned Starlab is organized according to a tree structure and most of the details of binary evolution are dealt with in a semi-analytical manner using the binary evolution portion of SeBa. This is described in some detail in Portegies Zwart & Verbunt (1996) and Portegies Zwart & Yungelson (1998). The influence of bodies beyond some given radius outside the binary system can usually be treated as a perturbation to the semi-analytics. If bodies come too close the orbits have to be integrated explicitly (which drastically slows down computation).

In order to keep the parameter space small our simulations include no primordial binaries (also in order to reduce computation time) so we only need to trace the evolution of the binaries that form as a result of dynamics. The basic distribution of SeBa is fully capable of doing this with no modification.

3.1.3 Our Modifications

Starlab creates an initial snapshot by first creating a set of nodes according to an equilibrium model (e.g. a Plummer model) and then adding physical properties to these nodes with various subroutines. In particular a mass function can be added to a snapshot by means of the routine *makemass* which gives each node a mass chosen from a weighted probability function. A standard power-law mass function $\frac{dN}{dM} = cM^{-(1+x)}$ gives a mass to each node using the prescription:

$$M = M_l \left[\left(\left(\frac{M_{up}}{M_l} \right)^{(1+x)} - 1 \right) P + 1 \right]^{\frac{1}{1+x}}$$

where M_l and M_{up} are the lower and upper limits on the mass function and P is a random number between zero and one. The mass function prescribed by D’Antona & Caloi (2004) is a broken power law and takes the form:

$$\frac{dN}{dM} = \begin{cases} c_1 M^{-(1+\alpha)} & \text{if } M \leq M_B \\ c_2 M^{-(1+\beta)} & \text{if } M > M_B \end{cases}$$

It is represented graphically in Figure 3.2 for various choices of the exponents α and β and of the break mass M_B (c_1 and c_2 are simply normalization constants). This is a non-standard mass function which produces a strong enhancement in $3 - 5M_{\odot}$ stars and cannot be reproduced by any of the stan-

standard Starlab prescriptions. We had to encode this IMF ourselves by adding a function to the *makemass* routine which gives nodes a mass following a more complicated prescription.

First we fix the constants c_1 and c_2 by the number of RHB stars in NGC 2808, the specific choice of M_B , α and β and the criterion $c_1 M_B^{-(1+\alpha)} = c_2 M_B^{-(1+\beta)}$. This yields:

$$c_1 = \frac{dN}{dM} \Bigg|_{M_{RHB}} M_{RHB}^{-(1+\alpha)} \quad c_2 = c_1 M_B^{(\beta-\alpha)}$$

We can then calculate the number of stars in the α and β regimes:

$$N_\alpha = c_1 \frac{M_B^{-\alpha} - M_l^{-\alpha}}{-\alpha} \quad N_\beta = c_2 \frac{M_{up}^{-\beta} - M_B^{-\beta}}{-\beta}$$

The mass for an individual node is then generated using the prescription:

$$M = \begin{cases} M_l [(((\frac{M_B}{M_l})^{-\alpha} - 1) P_{mf} + 1)^\alpha] & P_{reg} \leq \frac{N_\alpha}{N} \\ M_B [(((\frac{M_{up}}{M_B})^{-\beta} - 1) P_{mf} + 1)^\beta] & P_{reg} > \frac{N_\alpha}{N} \end{cases}$$

where P_{reg} and P_{mf} are random numbers between zero and one and which determine respectively the mass regime a star will be in (α or β) and what its mass in that regime will be. This mass-function is defined entirely by the choice of α , β and M_B and produces the needed enhancement in high-mass stars. As a sanity check we have produced a Salpeter mass function (a standard power-law where $x = 1.35$) by inputting $\alpha = \beta = 1.35$ into the prescription and choosing M_B randomly. The results are identical as shown in Figure 3.3 and confirm that our new IMF prescription is accurate.

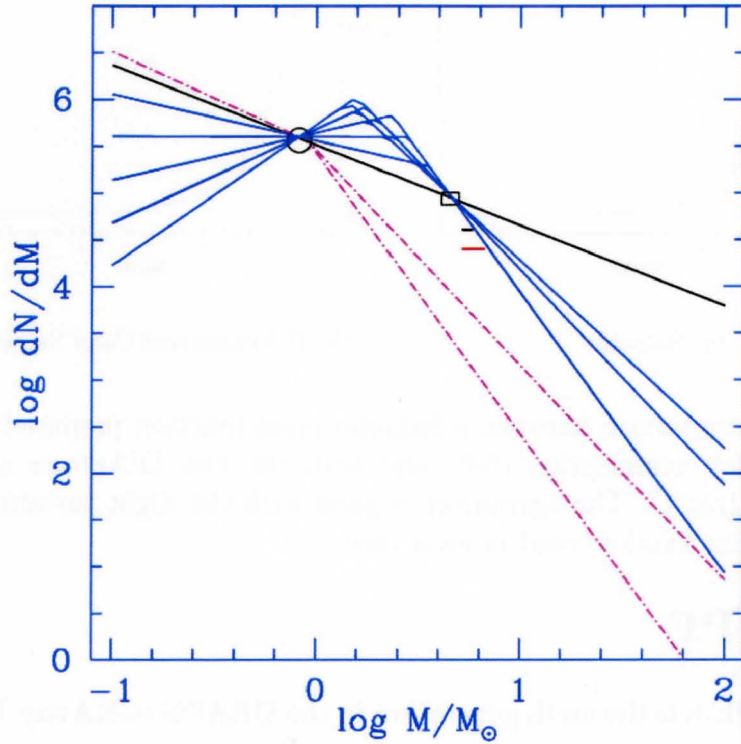


Figure 3.2 The D'Antona and Caloi mass function for various choices of α , β and M_B in blue. Two Kroupa mass functions (Kroupa, 2001) are shown in pink for comparison. The circle representing the number of RHB stars (565) and the square representing the number of BHB stars (401) in NGC 2808 are the constraints that the mass function must fit under the (unrealistic) D'Antona & Caloi (2004) assumption that one first-generation $3-5M_{\odot}$ AGB star produces exactly one second-generation BHB star. The straight line is the unique mass function where $\alpha = \beta = -0.14$. (D'Antona & Caloi, 2004)

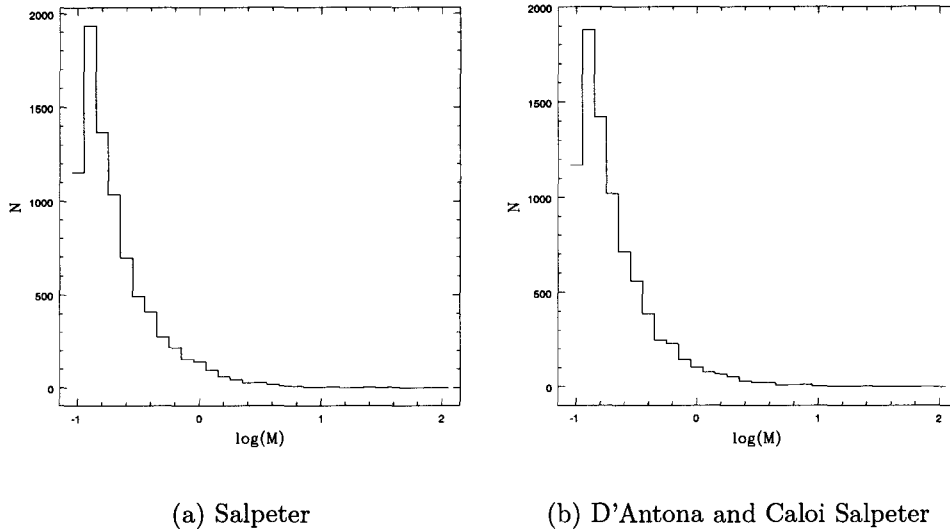


Figure 3.3 A comparison between a Salpeter mass function prepared with the standard Starlab prescription (left) and with the new D’Antona and Caloi mass function (right). The agreement is good with the slight variations being due to a different random seed in each case.

3.2 GRAPE

The GRAPE-6 is the sixth generation in the GRAPE (GRAvity PipelinE) series of special purpose gravitational accelerators (Makino (2001), Makino et al. (2003)). The GRAPE can provide several order-of-magnitude accelerations in direct N-body calculations over a standard computer. From the perspective of the simulator and the host computer the GRAPE acts as a black box to accelerate the Hermite predictor-corrector scheme. The N-body code passes the positions, velocities and masses of a set of particles and the GRAPE passes back accelerations, jerks and potentials. Starlab is specifically designed to make full use of GRAPE acceleration. Physically a GRAPE is a cluster of purpose-built integrated-circuit chips. At McMaster we have the GRAPE-6A (the micro or baby-GRAPE) version which consists of a single board with two

GRAPE chips on it. It plugs into a standard PCI slot in a desktop computer (given sufficient space in the computer case for the heat sink). A single baby-GRAPE provides speeds of up to 130 Gflops for N-body systems of up to $\sim 10^4$ particles (Fukushige et al., 2005). GRAPE-6A boards can also serve as modules out of which larger clusters can be built. The largest GRAPE-6 clusters commercially available contain 32 chips and can provide accelerations of several Tflops for larger values of N (Makino et al., 2003) but suffer from stability issues. We have found the baby-GRAPE to be more than sufficient for our needs.

Bibliography

D'Antona, F. & Caloi, V. 2004, ApJ, 611, 871

Eggleton, P. P., Fitchett, M. J., & Tout, C. A. 1990, ApJ, 354, 387

Eggleton, P. P., Tout, C. A., & Fitchett, M. J. 1989, ApJ, 347, 998

Fukushige, T., Makino, J., & Kawai, A. 2005, PASJ, 57, 1009

Kroupa, P. 2001, MNRAS, 322, 231

Makino, J. 1991, ApJ, 369, 200

Makino, J. 2001, in ASP Conf. Ser. 228: Dynamics of Star Clusters and the Milky Way, ed. S. Deiters, B. Fuchs, A. Just, R. Spurzem, & R. Wielen, 87–88

Makino, J. & Aarseth, S. J. 1992, PASJ, 44, 141

Makino, J., Fukushige, T., Koga, M., & Namura, K. 2003, PASJ, 55, 1163

McMillan, S. L. W. 1986, ApJ, 307, 126

Portegies Zwart, S. F., McMillan, S. L. W., Hut, P., & Makino, J. 2001, MNRAS, 321, 199

Portegies Zwart, S. F. & Verbunt, F. 1996, A&A, 309, 179

Portegies Zwart, S. F. & Yungelson, L. R. 1998, A&A, 332, 173

Tout, C. A., Aarseth, S. J., Pols, O. R., & Eggleton, P. P. 1997, MNRAS, 291,
732

Wiersma, R., Sills, A., & Portegies Zwart, S. 2006, ApJ, 637, 838

Chapter 4

Method

We use direct N-body methods to model a globular cluster in order to investigate dynamics in two scenarios: a top heavy IMF and the addition of a second generation of star-formation in an already dynamically evolved N-body system. We will compare our work mostly with the results of canonical simulations although we will try to present some observable results as well. We will use Starlab and the GRAPE to realize the models and the new D’Antona and Caloi IMF described in Chapter 3 to generate the top-heavy IMF. There are several choices to be made in the detailed implementation of our project: the exact parameters of the IMF must be constrained, a method of adding the second generation must be developed and diagnostic parameters must be chosen.

4.1 Choice of IMF Parameters

The D’Antona and Caloi mass function is specified by three parameters: α , β and M_B . There are many choices for these parameters which provide the requisite helium enhancement and indeed D’Antona & Caloi (2004) con-

sider a set of realizations within the parameter range: $0.90M_{\odot} \leq M_B \leq 3.80$, $-2.5 \leq \alpha \leq 0.0$ and $-0.14 \leq \beta \leq 3.00$. All of these choices yield a system significantly (between two to five times) more massive than the current mass of NGC 2808 ($1.6 \times 10^6 M_{\odot}$). In order to produce the least extreme scenario possible we choose the parameters that produce the lowest total mass: $\alpha = -0.50$, $\beta = 3.00$ and $M_B = 3.80$ corresponding to $M_{total} = 3.10 \times 10^6 M_{\odot}$. It is possible that a more massive IMF would have a stronger effect on cluster evolution but we consider our choice to be the least physically unreasonable. It is also worth noting that according to D’Antona & Caloi (2004) this IMF produces 4.13×10^4 neutron stars and 1.59×10^3 black holes, on par with on the number found by the same authors for a more conventional Kroupa IMF of a similar initial mass. Any other choice of parameters would produce many more compact remnants. Thus on the basis of stellar populations this also seems to be the least extreme choice. Choosing the most conservative implementation has the added advantage that if unreasonable results are produced more extreme implementations can be ruled out also. By contrast, if we produce unreasonable results in a more extreme simulation, we have no way of ruling out less extreme results and thus it is most efficient to consider the least extreme scenario first.

4.2 The Evolution of the First Generation

We implement our first generation using 4096 particles distributed according to a Plummer distribution function (Plummer, 1911) and using the lowest-mass D’Antona and Caloi IMF. We choose 4096 particles because the evolu-

tion of such a system takes a reasonably short time and we are able to produce several simulations efficiently. Furthermore, the second generation will add an additional ~ 8000 particles giving a total simulation size of ~ 12000 particles. Such a simulation can still be performed in a reasonable period of time but, according to the results of Giersz & Heggie (1996) is beyond the realm of small number statistics. We follow Hurley et al. (2005) in using a Plummer model for the reasons described in Chapter 2. We also produce a similar simulation using a Salpeter IMF for comparison purposes.

Once the initial cluster has been generated we allow it to evolve in Starlab for a time corresponding to 200 Myrs. This is the time necessary for all stars in the range of $3 - 5M_{\odot}$ to reach the AGB phase and enrich the ISM with helium. During this initial evolution the cluster undergoes mass loss due to stellar evolution and it is from this ejecta that the second generation forms. According to Gnedin et al. (2002) the characteristic terminal velocity for AGB winds is $\sim 15kms^{-1}$ whereas the escape velocity for a cluster of the mass of NGC 2808 is on the order of $60kms^{-1}$ in the core and $40kms^{-1}$ at the half mass radius. It thus seems plausible that a large fraction of the mass lost by AGB stars will in fact be retained as gas by the cluster. To model this we assume that the retention fraction is 100% and model it with a static, analytic Plummer potential $\phi(r) = -\frac{GM}{\sqrt{r^2+a^2}}$, added before the start of the simulation. M is matched to the mass lost during the first generation (we evolve the cluster without the potential to calculate M) and a is the characteristic scale radius of the Plummer model that will be used to initialize the second generation. The assumption of 100% retention is not necessarily realistic but, provided the cluster has made no transits through the galactic disk in its first 200 Myr, the

retention fraction is likely to be high and assuming 100% retention will allow us to conserve mass when adding the second generation. Significantly more unrealistic is the approximation of a static external potential of constant mass throughout the course of the simulation. More realistically we should add gas to the simulation locally where it is lost by the stars and the mass of the potential should evolve in step with the mass-loss. Not adding the gas locally is not a problem since at 15kms^{-1} the gas crossing time at the viral radius is ~ 3 Myr (on the order of a single timestep) and the particle crossing time is ~ 8.5 Myr (about three timesteps). Thus we would expect gas produced locally to be quickly distributed throughout the cluster. In order to examine the effect of adding too much mass early we consider the Lagrangian radii for one of our first-generations in Figure 4.1.

The main effect of this potential is to keep the cluster from expanding due to mass-loss as demonstrated by the smaller Lagrangian radii when the potential is introduced. This effect is seen in both the massive and overall Lagrangian radii which is a good indication that mass segregation has not been suppressed and two-body relaxation has not been affected. This is, in fact, exactly the same effect we would expect if we allowed the mass of the potential to evolve in step with the mass loss of the cluster and balance out the dissipation. The only qualitative effect not expected with the time-evolving potential is the sharp decrease in the first few timesteps of the cluster with the static potential. This is caused by having extra mass early before it has actually been lost by stars in the cluster. Since by the end of the run the cluster has evolved for about a half-mass relaxation time any unwanted dynamical effects this may have should be erased. Obviously a localized SPH treatment

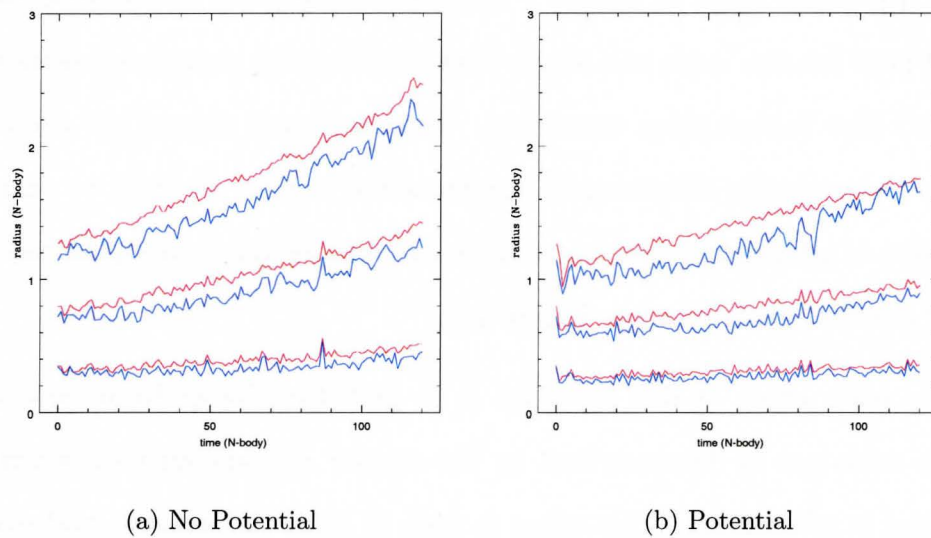


Figure 4.1 On the left are the Lagrangian radii for a cluster with a top-heavy IMF evolving for 200 Myr. On the right is the same cluster evolving for 200 Myr in a Plummer potential with a mass equal to the mass lost due to stellar evolution. From bottom to top we have the 10%, 50% and 75% Lagrangian radii. Red indicates the Lagrangian radii for the entire system, blue indicates the Lagrangian radii for stars in the most massive 10%.

of the ejecta or a time-evolving potential would be preferable but the difference would be in details rather than in overall effect. An SPH treatment is beyond the scope of this project and the incorporation of a time-evolving potential into Starlab would be rather difficult. Since we are only interested in the details of the dynamics after the second generation is added our approximation will be sufficient.

4.3 The Second Generation

In order to implement the second generation we must find some way to add stars to a pre-existing snapshot. The easiest way to implement this in Starlab is to create a separate snapshot using the parameters characterizing the second generation and then combining this snapshot with the output snapshot from the first generation using the routine *merge_snaps*. We implement the second generation according to a Plummer model but with a Salpeter IMF (Salpeter is chosen for reasons outlined in Chapter 2). We choose the total mass of the Salpeter IMF to match the mass of the Plummer potential and hence the mass lost in our initial cluster. This implicitly implies 100% star formation efficiency. This assumption is almost certainly unrealistic but it is both in keeping with the spirit of the scenario proposed in D’Antona & Caloi (2004) and it allows us to conserve mass when adding the second generation (all of the Plummer potential mass is replaced by stellar mass). Furthermore, the actual star formation efficiency during galactic globular cluster formation is not known so to consider different star formation rates would vastly increase our parameter space without providing any particular physical insight. It

is also worth noting that in constraining our second generation by mass we allow the particle number to vary slightly between simulations. Since we are operating in the range insensitive to particle number this is not of concern. It is also important to note that Starlab uses Heggie units (Chapter 2) for its calculations and physical conversions in these units are dependant on the total mass and length scale of the system. For this reason we must carefully scale the second generation so that the physical units match those of the first generation. This is accomplished using Starlab's *scale* command. Once properly scaled we use the *merge_snaps* routine to combine the first and second generation snapshots into a single snapshot and manually remove the Plummer potential from the first generation. This procedure represents the conversion of a continuous gas potential into a generation of stars with the same total mass in one timestep (~ 1 Myr).

4.4 Evolution of the Combined Cluster

Once the combined cluster is prepared it is allowed to dynamically evolve in Starlab for as long as possible. During this phase mass from the cluster is no longer replaced (there is no Plummer potential) and the total mass of the system decreases due to stellar evolution. At least one initial half-mass relaxation time is necessary for dynamical stability to be achieved and any meaningful conclusions to be drawn. Several initial half-mass relaxation times are better in order to understand the long-term evolution. Core collapse, the phase of dynamical evolution where the cluster core density approaches infinity, occurs after ~ 15 initial half-mass relaxation times and simulations

of galactic globular cluster dynamics should reach this stage in order to fully describe the current population. Due to our initial parameters, after two to four half-mass relaxation times our clusters eject high-velocity neutron stars to well beyond the cluster radius. This is expected but it has the effect of reducing the timestep to zero and irrecoverably crashing the simulations. Two to four half-mass relaxation times are sufficient to understand initial trends in the cluster's evolution but without introducing a stripping radius we cannot push our simulations further than this. We are currently investigating the implementation of an appropriate stripping radius to remove the neutron stars once they have been ejected far enough so that we can evolve simulations up to and beyond core collapse.

During the evolution of the combined cluster we track both the Lagrangian radii for information on the spatial distribution of stars and the average mass at a given Lagrangian radii for information on mass segregation. We track velocity dispersions in order to gain further insight into the dynamical stability of the cluster. These parameters are largely unobservable and can only be compared to results from previous, canonical simulations. For observables we track the evolution of the mass function, the final stellar composition of the clusters and the final mass-to-light ratios. These parameters are concerned with stellar populations in globular clusters rather than their dynamics but they are observable properties that may help determine the validity of the two-generation globular cluster formation scenario.

4.5 Our Models

We consider six models with the initial parameters shown in Table 4.1. We run a Salpeter and a D’Antona and Caloi IMF without a second generation in order to determine the effect of a top-heavy IMF alone (SP and DC). We then run three simulations with a second generation of stars added after 200 Myr (the Cx5 family of simulations). Finally we present a model (C2.5) which was performed with an initial virial radius of 2.5 pc rather than 5.0 pc. It is not entirely clear what choice of physical concentration best represents the initial conditions of galactic globular clusters and since physical scaling of the system affects the concentration of the cluster and to some extent the shape of its potential the difference could be important. We try to constrain this effect with C2.5.

Simulation Parameters						
Run ID	1 st gen			2 nd gen		
	N	$M_{tot}(M_{\odot})$	$R_{vir}(\text{Pc})$	N	$M_{tot}(M_{\odot})$	$R_{vir}(\text{Pc})$
SP	8192	3051	2.5	-	-	-
DC	8192	18077	2.5	-	-	-
Ca5	4096	8982	5.0	8130	2900	5.0
Cb5	4096	9104	5.0	8350	3039	5.0
Cc5	4096	8778	5.0	8200	2900	5.0
C2.5	4096	8982	2.5	7700	2770	2.5

Table 4.1 The parameters used to initialize our eight simulations. The ID identifies the run. The total particle number, total mass and virial radius for each generation are given (the mass of the second generation matches the mass lost in the first).

Bibliography

D'Antona, F. & Caloi, V. 2004, ApJ, 611, 871

Giersz, M. & Heggie, D. C. 1996, MNRAS, 279, 1037

Gnedin, O. Y., Zhao, H., Pringle, J. E., Fall, S. M., Livio, M., & Meylan, G.
2002, ApJ, 568, L23

Hurley, J. R., Pols, O. R., Aarseth, S. J., & Tout, C. A. 2005, MNRAS, 363,
293

Plummer, H. C. 1911, MNRAS, 71, 460

Chapter 5

Results

We present an examination of the results of simulations described in Chapter 4. First we consider the results of simulations SP and DC in order to constrain the effect of the top-heavy IMF. We then explore the effect of adding a second generation to the D’Antona and Caloi IMF using the *Cx5* family of simulations. Finally we investigate the effect of concentration with simulation C2.5. In each case we examine dynamics and stellar properties separately.

5.1 The Top-heavy IMF (SP vs. DC)

Both of these simulations have a single generation with SP initialized according to a Salpeter IMF and DC initialized with a D’Antona and Caloi IMF. For ease of comparison we present our results in N-body units and give physical conversions in Table 5.1

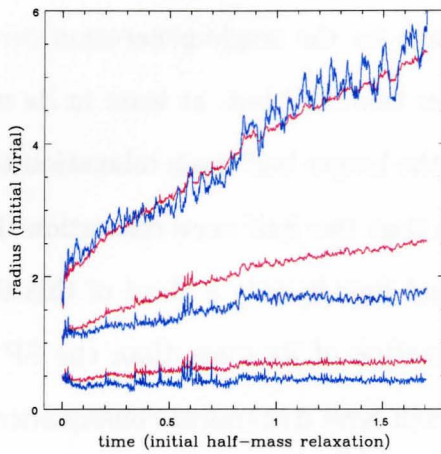
5.1.1 Dynamics

We give some of the physical parameters for the single-generation runs in Table 5.1. Note that SP is physically older than DC but, at least in its early phases, is less dynamically evolved due to the longer half-mass relaxation time. Indeed in ~ 3 Gyr SP has experienced less than two half mass relaxation times while DC has undergone between three and four in only a third of this time. The DC run also loses a much greater fraction of its mass than the SP run over a much shorter period of time. This will have dynamical consequences as shown by the Lagrangian radii in Figure 5.1 and the RMS velocity dispersion in Figure 5.2.

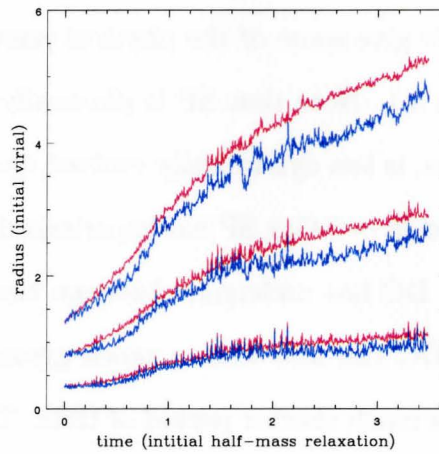
In each of Figure 5.1 and 5.2 the SP results are on the left and the DC results on the right. An important result from Figure 5.1 is that for SP the 10% and to some extent the 50% Lagrangian radii flatten off while in DC even the 10% Lagrangian radius continues to grow. This trend is repeated in Figure 5.2 where the RMS velocity for SP flattens rapidly and the DC RMS velocity continues to grow. A continuing increase in these parameters (particularly in the Lagrangian radii) is indicative of mass-loss reducing the potential well of the cluster and causing it to expand. Flattening on the other hand

Physical Parameters					
ID	$M_{in}(M_{\odot})$	% Lost	$R_v(\text{pc})$	$T_{RH}(\text{Myr})$	Final Age(My)
SP	3051.36	25.68	5.0	1760.6	3005.5
DC	18077.43	58.52	5.0	299.4	1043.4

Table 5.1 Column (1) gives the run ID, (2) is the initial mass of the system, (3) is the percent of mass lost during the simulation, (4) is the initial viral radius), (5) is the physical length of the N-body timestep, (6) is the initial half-mass relaxation time in N-body timesteps and (7) is the final age of the cluster in N-body timesteps.

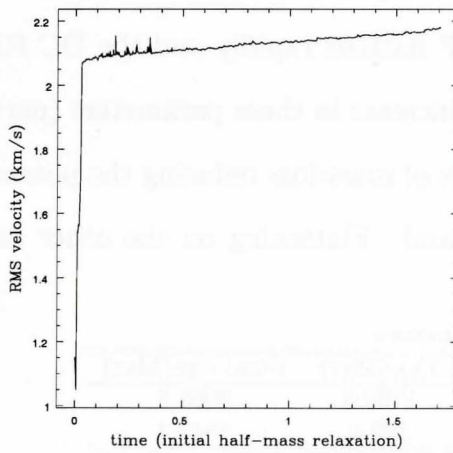


(a) Salpeter

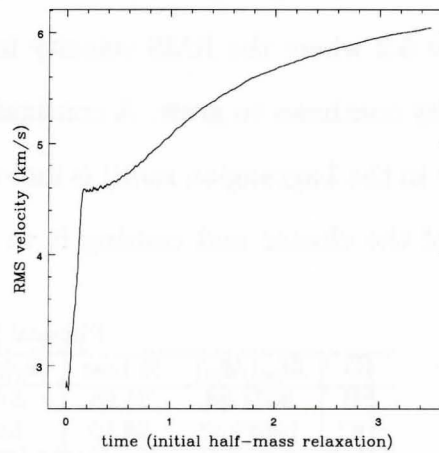


(b) D'Antona and Caloi

Figure 5.1 The evolution of the Lagrangian radii. From bottom to top: 10%, 50% and 75% Lagrangian radii. Red indicates the Lagrangian radii of all stars in the cluster, blue indicates Lagrangian radii for the most massive 10% of cluster members.



(a) Salpeter



(b) D'Antona and Caloi

Figure 5.2 RMS velocities calculated by inverting the total kinetic energy of the cluster members.

indicates evolution towards a state of long-term stability. It follows that SP is less affected by mass loss than DC where the dynamics are mass-loss dominated. The dynamical evolution of SP seems to be dominated by two-body relaxation as evidenced by mass segregation observed in the Lagrangian radii where the most massive stars (blue) have a different, more centrally concentrated distribution than the entire cluster population (red). Mass segregation can also be observed in the average masses at different Lagrangian radii (as in Chapter 2) plotted in Figure 5.3.

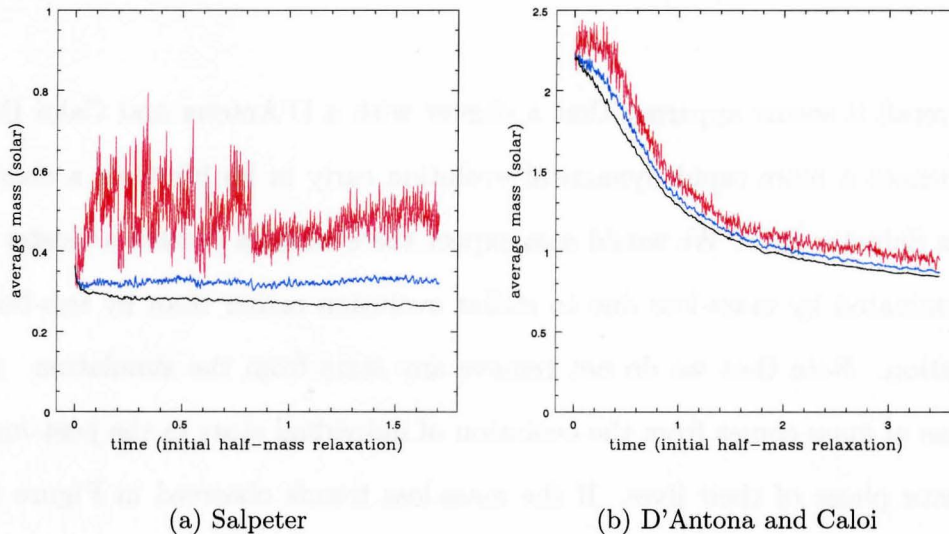


Figure 5.3 The average mass at the 10% (red), 50% (blue) and 75% (black) Lagrangian radius.

By looking at the distance between massive and overall Lagrangian radii and the difference in average masses at different Lagrangian radii it becomes apparent that mass segregation is more extreme in the SP case. Since mass segregation is a two-body relaxation effect this indicates that two-body relaxation is the dominant mechanism driving dynamical evolution in SP. Possible

reasons for the difference between SP and DC include a broader spread of masses in DC reducing the effect of a few massive stars on overall parameters, the dominance of mass-loss in DC (emphasized further by the strong evolution of the average masses in Figure 5.3) and the greater inertia of the more massive stars making two-body encounters less effective at disrupting the entire DC system.

Overall it seems apparent that a cluster with a D’Antona and Caloi IMF experiences a more rapid dynamical evolution early in its life than a cluster with a Salpeter IMF. We would also expect the evolution of such a cluster to be dominated by mass-loss due to stellar evolution rather than by two-body relaxation. Note that we do not remove any stars from the simulation. All the loss of mass comes from the evolution of individual stars in the post-main sequence phase of their lives. If the mass-loss trends observed in Figure 5.1 were to continue the DC cluster would dissipate entirely in under a Hubble time, probably before reaching core collapse. It is likely, however, that the rate of mass-loss will be significantly reduced at later stages of cluster evolution. This is because the high-mass stars responsible for the high rate of initial mass-loss will have evolved to their stable, remnant stage and the remaining low-mass stars lose mass at a much slower rate. If this is the case then the cluster will stabilize and cease to expand so radically. Longer simulations will be needed to confirm this.

5.1.2 Stellar Population

Both simulations were initiated with 100% main sequence stars and allowed to evolve from there. We investigate the evolution of the stellar populations by considering the number of stars by type (Table 5.2) and by studying the evolution of the mass function (Figure 5.4).

Final Stellar Population				
Type	SP		DC	
	#	%	#	%
Main Sequence	7966	97.24	4319	52.72
Hertzsprung Gap	3	0.0366	11	0.1342
Sub Giants	12	0.1465	1	0.0122
Horizontal Branch	3	0.0366	73	0.8911
C-O White Dwarfs	176	2.148	3527	43.05
Neutron Stars	23	0.2808	131	1.599
Black Holes	9	0.1099	4	0.0488
<i>M/L</i>	1.240		0.225	

Table 5.2 The final stellar population of the clusters. Column (1) gives the type of stars, (2) and (4) give the number of each type and (3) and (5) give the percentage by number that each type contributes. The last row gives mass-to-light ratios. For more information on these types of stars see Chapter 3

Table 5.2 indicates that SP undergoes minimal stellar evolution and retains almost all of its main sequence stars whereas DC evolves dramatically and quickly becomes dominated by stellar remnants. This is expected since 1 Gyr is ample time for a large number of the high-mass stars produced by the top-heavy IMF to expend their fuel and become white dwarfs. It is interesting to note that the mass-to-light ratio for DC is much lower than that of SP.

In Figure 5.4 we show the evolution of the mass function for both clusters. The strong peak in the DC case consists mainly of C-O white dwarfs which at this age are still quite bright. It is also worth noting that the DC mass function peaks at a higher mass than the SP mass function even after experiencing a

gigayear of stellar evolution. Stars in the DC peak are either more massive main-sequence stars or young white dwarfs, both of which are quite bright. This naturally leads to a lower mass-to-light ratio in DC than in SP.

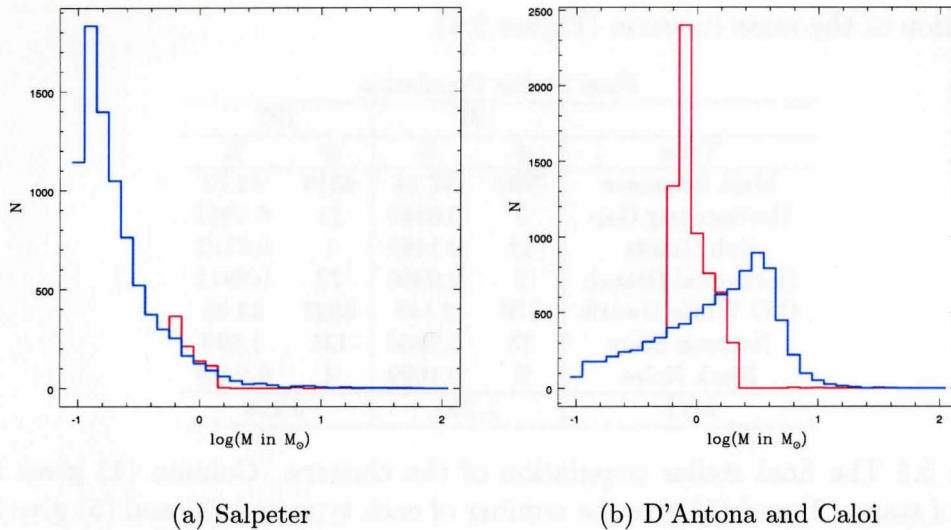


Figure 5.4 The evolution of the mass functions. The initial mass functions are in blue, the final in red. The strong peak in (b) is composed mainly of C-O white dwarfs.

We expect the mass-to-light ratio for DC to grow rapidly as these stars evolve past their nuclear burning phase and to finally exceed that of SP but a longer simulation would be needed to confirm this. Figure 5.4 also confirms that the stellar population of DC undergoes radical evolution in the first Gyr of its life while SP changes very little in a much longer period of time. Overall we expect the later stages of a cluster with a pure D'Antona and Caloi IMF to be dominated by white dwarfs to a much greater extent than a cluster with a Salpeter IMF. Such differences in populations could be observable in future studies and would be a smoking gun for a top-heavy IMF.

5.2 The Second Generation (Ca5, Cb5 and Cc5)

SP and DC are now used for comparison with the Cx5 family of models. We present three simulations in this section, each of which is prepared in an identical way but with a different random seed. The Cx5 family of simulations consists of D’Antona and Caloi IMFs evolved for 200 Myr after which second generation prepared according to a Salpeter IMF added. Again the results are reported in N-body units with physical parameters given in Table 5.3.

Physical Parameters					
ID	$M_{in}(M_{\odot})$	% Lost	$R_v(\text{pc})$	$T_{RH}(\text{Myr})$	Final Age(Myrr)
Ca5	8907	42.64	5.0	838.3	2275.8
Cb5	9098	41.88	5.0	843.0	1809.6
Cc5	8777	38.19	5.0	816.0	1204.5

Table 5.3 Column (1) gives the run ID, (2) is the initial mass of the system, (3) is the percent of mass lost during the simulation, (4) is the initial viral radius, (5) is the physical length of the N-body timestep, (6) is the initial half-mass relaxation time in N-body timesteps and (7) is the final age of the cluster in N-body timesteps.

It is worth noting that these parameters are for the combined system once the second generation has been added. This means that the stars of the first generation are 200 Myr older than the reported system age.

5.2.1 Dynamics

The N-body timestep of the Cx5 systems is still physically shorter than the timestep for the SP system but since the N-body half-mass relaxation time is longer than that of DC the physical half-mass relaxation times of the Cx5 models and SP are actually comparable (if differences in number are taken

into account). Indeed the initial half-mass relaxation time for a Salpeter mass function with 12000 particles, if calculated analytically according to the Spitzer prescription, is ~ 880 Myr, almost identical to the *Cx5* models. It is also worth noting that although mass-loss for the *Cx5* models is more significant than for SP case it is not as severe as in the DC case.

When we examine the Lagrangian radii (Figure 5.5) and the RMS velocities (Figure 5.6) to gain more insight into how this affects the dynamical evolution of the system we find results intermediate between the SP and DC case. The growth in the Lagrangian radii is still present but at a lower level and the 10% radii appear to become flat towards the end of the simulations. Likewise there is still a growth in the RMS velocity but overall the profiles are much flatter than in the DC case. Figures 5.5 and 5.7 show signs of mass segregation almost as strong as for the SP model. In particular reverse mass segregation at the 75% radius is apparent in Ca5, Cb5, Cc5 and SP but not in DC.

Stronger mass segregation suggests that two-body relaxation is more significant in the two-generation clusters than the the DC cluster alone. This is due partly to the introduction of many low-mass stars which will be strongly affected by two-body scattering, and partly to the introduction of the second generation which has made the system denser and hence increased the frequency of two-body interactions.

Overall the dynamics of the *Cx5* family of clusters seem to be intermediate between a pure D'Antona and Caloi IMF and a Salpeter IMF but overall closer to Salpeter behaviour. That the results should be intermediate between the two IMFs is not surprising (we are combining one of each) but the tendency

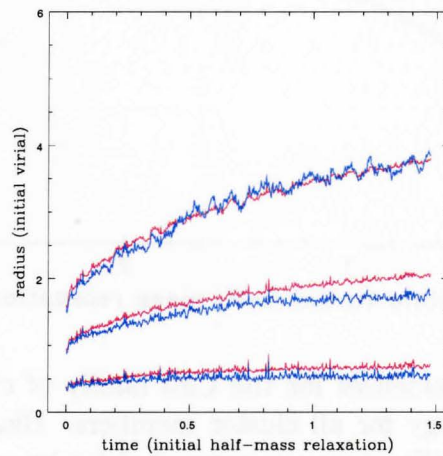
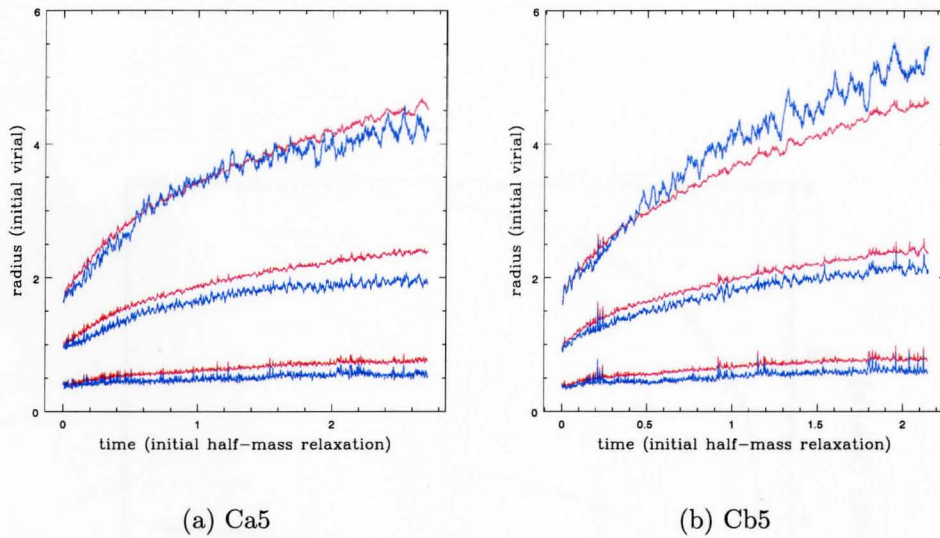


Figure 5.5 The evolution of the Lagrangian radii for the second generation clusters. From bottom to top: 10%, 50% and 75% radii. Red indicates overall Lagrangian radii, blue indicates Lagrangian radii for the most massive 10% of cluster members.

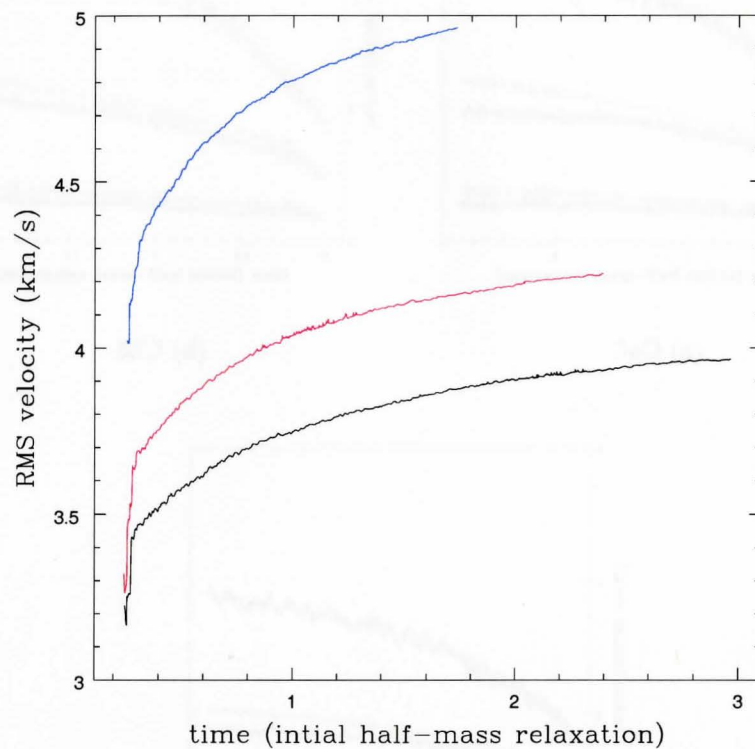
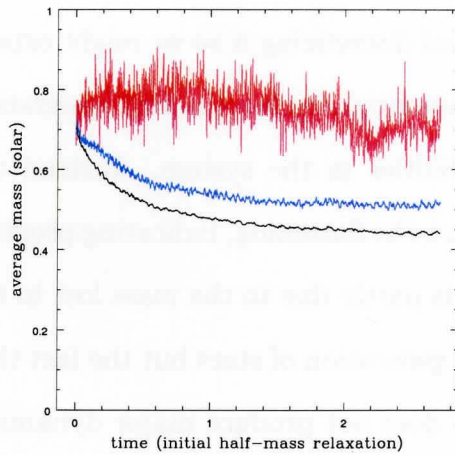
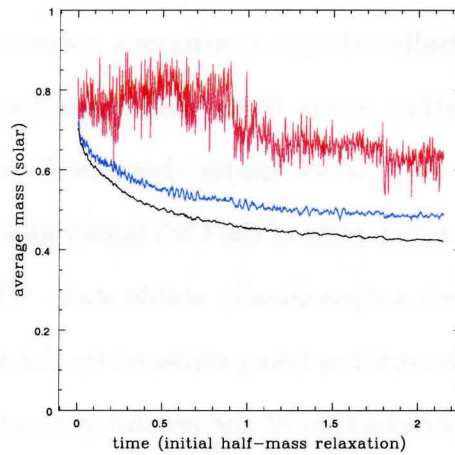


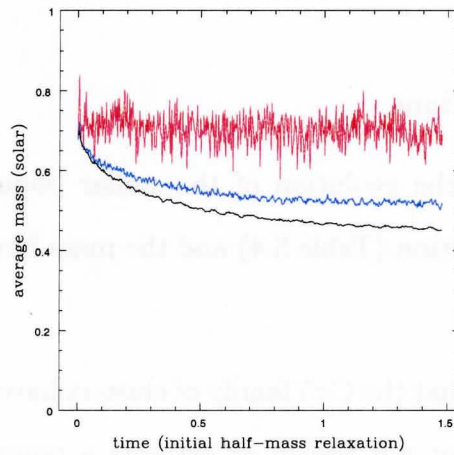
Figure 5.6 The RMS velocities for the *Cx5* family of clusters derived by inverting the kinetic energy for all cluster members. Black is Ca5, red is Cb5 and blue is Cc5. The differences are accounted for by variations in age, total mass and different mass-loss in the first generation due to different random seeds in the *makemass* routine.



(a) Ca5



(b) Cb5



(c) Cc5

Figure 5.7 The average mass at the 10% (red), 50% (blue) and 75% (black) Lagrangian radii for the two-generation clusters.

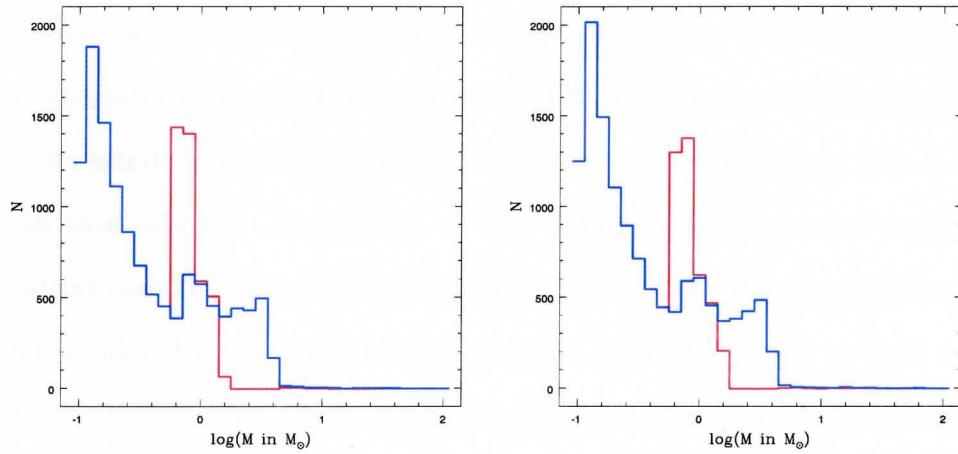
towards the Salpeter is interesting, suggesting number rather than mass is the dynamically dominant factor (Table 4.1). More unexpected is that there is no evidence that the $Cx5$ family of clusters are dynamically unstable. We are essentially taking a continuous potential and discretizing it so we might expect the rather severe disruption of the local potential around the first generation stars to produce major dynamical instabilities in the system. Instead the Lagrangian radii of the $Cx5$ family all seem to be flattening, indicating progress towards a dynamically stable state. This is partly due to the mass lost in the first generation being replaced by the new generation of stars but the fact that the introduction of the second generation does not produce major dynamical instabilities in the cluster is hardly intuitive. The implication that N-body systems are robust against such disruptions is a very interesting result!

5.2.2 Stellar Populations

Again we consider the evolution of the stellar population by examining the final stellar composition (Table 5.4) and the mass function evolution (Figure 5.8).

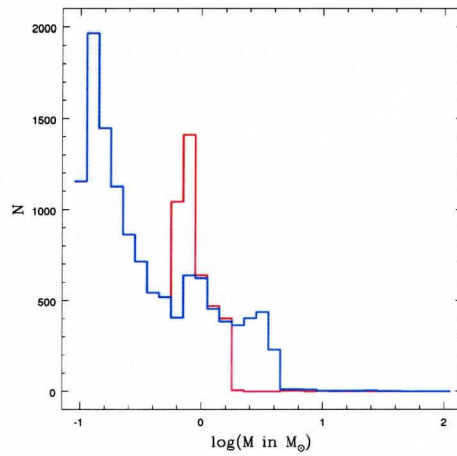
Table 5.4 indicates that the $Cx5$ family of clusters have a significant fraction of C-O white dwarfs but not nearly as extreme a population as DC had in a shorter time. It is also apparent from Figure 5.8 that although the high mass portion of the spectrum is significantly altered the evolution of the mass function in the low-mass range is negligible.

Both of these effects can be attributed to the IMF's evolving separately and the result then averaged over the entire system. It is interesting to note



(a) Ca5

(b) Cb5



(c) Cc5

Figure 5.8 The evolution of the mass functions. The initial mass function is shown in blue, the final in red.

the double peak in the evolved mass functions. The low-mass peak contains the second-generation stars, many of which would still be hydrogen burning after a Hubble time. The high mass peak contains the white dwarf remnants produced by the first generation, most of which would have a low luminosity at current globular cluster ages. If they exist the white dwarfs in the high mass peak should be revealed with deep observations of galactic globular clusters. If they are not the top-heavy IMF will be disfavoured. We also note higher mass-to-light ratios in the *Cx5* family of clusters than the DC case (although not as high as in the SP case). Again in clusters aged for a Hubble time we would expect a higher mass-to-light ratio than is produced by a Salpeter IMF due to the cooling of the white dwarfs from the first generation.

5.3 The Effect of Length (C2.5)

As mentioned in Chapter 4 the proper choice for a physical length scale is unclear. We use this simulation to investigate the effects of a different choice of length scale, comparing it to SP and DC as well as the *Cx5* family of simulations. The preparation of this simulation is identical to the *Cx5* family except that it has a virial radius (and thus a length unit) of 2.5 pc rather than 5.0 pc. Physical units are given in Table 5.5.

The timescale for dynamical evolution in this cluster is very short, on the order of DC in physical units, and it is our youngest cluster. That the half-mass relaxation time is shorter than the *Cx5* family is to be expected since the reduction in the length unit reduces the physical crossing time. The

Final Stellar Population						
Type	Ca5		Cb5		Cc5	
	#	%	#	%	#	%
Main Sequence	9643	78.87	10024	80.54	10122	82.32
Hertzsprung Gap	15	0.1227	12	0.0964	8	0.0651
Sub Giants	72	0.5889	60	0.4821	78	0.6344
Super Giants	1	0.0082	1	0.0080	0	0.0
Horizontal Branch	12	0.0982	25	0.2009	33	0.2684
C-O White Dwarfs	2399	19.62	2229	17.91	1959	15.93
Neutron Stars	72	0.5889	83	0.6669	89	0.7238
Black Holes	12	0.0982	12	0.0964	7	0.0569
<i>M/L</i>	0.545		0.632		0.544	

Table 5.4 The final stellar population of the clusters. Column (1) gives the type of stars, (2) and (4) give the number of each type and (3) and (5) give the percentage by number that each type contributes. The last row gives mass-to-light ratios.

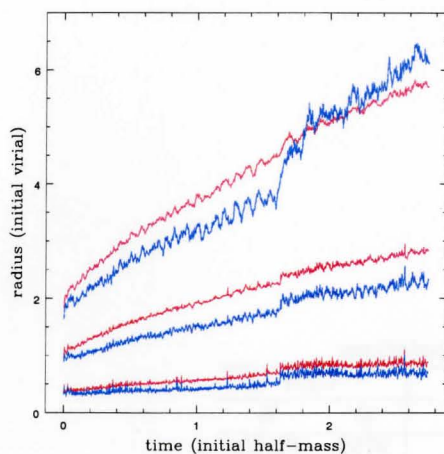
Physical Parameters					
ID	$M_{in}(M_{\odot})$	% Lost	$R_v(\text{pc})$	$T_{RH}(\text{Myr})$	Final Age(Myrr)
C2.5	8982	37.26	2.5	283.8	772.9

Table 5.5 Column (1) gives the run ID, (2) is the initial mass of the system, (3) is the percent of mass lost during the simulation, (4) is the initial viral radius, (5) is the timestep in physical units, (6) is the initial half-mass relaxation time in N-body timesteps and (7) is the final age of the cluster in N-body timesteps.

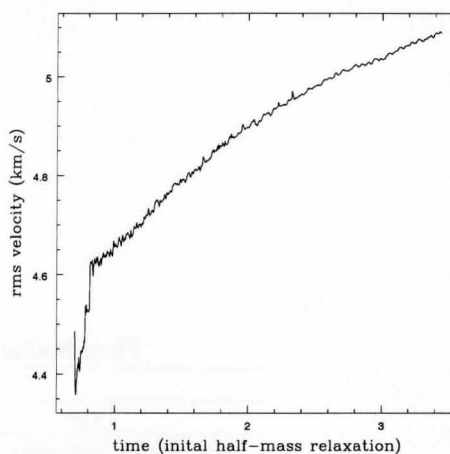
concentration of the cluster in physical space would also tend to increase the number of two-body interactions and thus accelerate two-body relaxation.

Figure 5.9 indicates that two-body relaxation and mass-loss are both important factors in the evolution of this cluster. All of the Lagrangian radii increase as a result of mass loss (although the growth of the 10% radius is less pronounced than in the DC case). The RMS velocity also increases steadily, again indicating that mass-loss has a significant effect. We do, however see characteristic two-body effects such as mass segregation from the Lagrangian radii and average mass profiles. We also see a jump in the Lagrangian radii at timestep ~ 700 caused by three-body scattering of a massive binary system from the cluster core, a characteristic two-body effect. The concentration seems to have made two-body effects more important while not reducing the effect of mass-loss on the cluster. We also examine the stellar populations in Figure 5.9 and Table 5.6 and find a less extreme degree of the behaviour seen in the *Cx5* models. Because C2.5 has the same IMF as the *Cx5* family of models but is physically younger and thus has a less evolved stellar population this result is not unexpected.

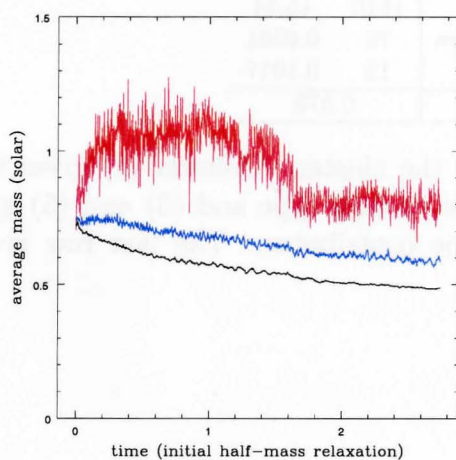
Overall the C2.5 model seems to be more unstable to two-body effects than the *Cx5* models but is otherwise similar. The Lagrangian Radii and the RMS velocity do not display the flattening that occurs in the later phase of the *Cx5* models. This may simply be due to the younger age where mass-loss is more rapid so no conclusions about mass-loss induced dissipation can be formed.



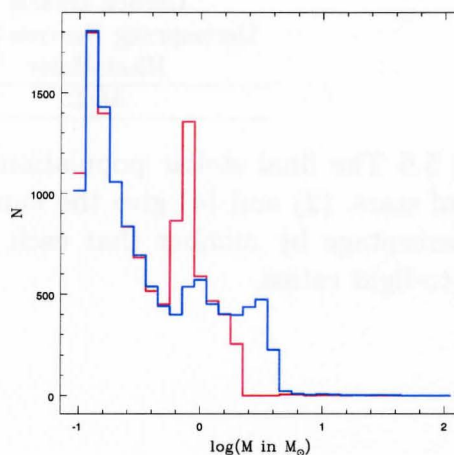
(a) Lagrangian Radii



(b) RMS velocity



(c) Average Masses



(d) IMF Evolution

Figure 5.9 Dynamical properties for the cluster with modified length scale. Colours and units are the same as for 2nd generation cluster plots.

Final Stellar Populations		
Type	C2.5	
	#	%
Main Sequence	9759	82.73
Hertzsprung Gap	13	0.1102
Sub Giants	66	0.5595
Super Giants	0	0.0
Horizontal Branch	61	0.5171
Carbon Dwarfs	1810	15.34
Hertzsprung Neutron Stars	75	0.6381
Black Holes	12	0.1017
<i>M/L</i>	0.370	

Table 5.6 The final stellar population of the cluster. Column (1) gives the type of stars, (2) and (4) give the number of each type and (3) and (5) give the percentage by number that each type contributes. The last row gives mass-to-light ratios.

Chapter 6

Discussion and Conclusions

In this thesis we have considered the dynamical effect of a second generation of star formation in globular clusters in order to better understand the self-enrichment scenario. In particular we have studied the implications of adding a dynamically unevolved generation of stars with a Salpeter IMF to a dynamically evolved generation of stars with a top-heavy IMF. We have found that such a two-generation cluster is no less dynamically stable than a single-generation cluster with a Salpeter IMF but has a different stellar population. In this section we comment on the results of our simulations and try to link these results with potential observations. We consider the prospects for AGB stars in the context of the self-enrichment scenario and summarize the results of our work.

6.1 Discussion of Results

For the pure D’Antona and Caloi IMF we see very rapid dynamical evolution dominated by mass-loss. Given the short timescale of dynamical evolution, we find that the early dynamical evolution of clusters with a pure

D’Antona and Caloi IMF is far more rapid than for clusters with a Salpeter IMF. We also note that clusters with a top-heavy IMF are dominated by extensive mass-loss and consequently expand quickly in their early phases. This result is consistent with previous work on top-heavy IMFs (Fukushige & Heggie (1995), Giersz (2001) and Joshi et al. (2001)). Since the high-mass stars responsible for the extreme mass-loss evolve to their remnant phase quickly, we expect the rate of mass-loss to decrease dramatically at later times. Longer simulations will be needed to confirm this.

In the case of a D’Antona and Caloi IMF with a second generation we have a more interesting dynamical situation. These simulations experience significant mass-loss in comparison to a Salpeter single-generation model but they appear to stabilize more quickly and experience stronger two-body relaxation effects than would a top-heavy IMF single-generation model. That the mass-loss is stronger than for a Salpeter IMF is not surprising since there are still many massive stars remaining from the first population. It is also expected that the mass-loss would be less than in the pure D’Antona and Caloi case since the stars of the second generation will evolve more slowly and dilute the effect of mass-loss in the first generation for the cluster as a whole. It is also worth noting that the very high mass stars in the first generation will have evolved past the mass-loss stage in the first 200 Myr and will not contribute to mass-loss in the second generation phase. The introduction of the second generation does not seem to produce any dynamical instabilities in the cluster and indeed these clusters seem no more unstable than those with a single-generation and a standard IMF. This result is somewhat unexpected since the discretization of the smooth Plummer potential upon introducing the

second generation will change the local potential rather severely. Intuitively one might expect this to lead to some sort of dynamical instability. This dynamical stability in the face of a second generation is an interesting result. The two-generation clusters also seem to have dynamical timescales similar to those in Salpeter IMF systems and should be in the same state of dynamical evolution at the same physical ages. Overall, except for being of higher mass and thus having a somewhat higher RMS velocity, the two generation clusters seem to be dynamically indistinguishable from a single-generation cluster with a Salpeter IMF in most observable ways. The null result comes as a great surprise to us and we consider it to be very significant.

When considering stellar populations we note significant differences between the single-generation and two-generation clusters. In particular the two-generation clusters have an order of magnitude larger number of intermediate-mass stellar remnants at a younger age than a standard single-generation cluster. Most of these remnants are C-O white dwarfs which would easily survive 10-12 Gyr and should still be observable (e.g Hansen (1999), Hansen et al. (2002)) although at a lower luminosity than earlier in their lives. Since mass segregation in the two-generation clusters is the same as in single-generation simulations and since white dwarfs are not preferentially scattered out of standard simulations we would not expect these bodies to be dynamically removed from the two-generation clusters. Rather we expect that these dark remnants would remain in the cluster until it dissipates after core collapse. Thus, although the dynamics of single-generation Salpeter IMF clusters and two-generation clusters appear identical, their stellar populations could differ significantly.

6.2 Observational Prospects

Since single-generation and two-generation clusters experience similar dynamical evolution, there are probably no observations of dynamical properties that will discriminate between them. The one exception to this might be the total mass. Two-generation clusters with a top-heavy IMF in the first generation are initially more massive than a cluster with the same number of particles but a Salpeter IMF. Thus dynamical properties that are affected by mass, such as velocity dispersions, may help determine the origin of a cluster when compared with observations of other systems. It is worth noting, however, that a two-generation cluster will lose a larger fraction of its mass than a single-generation cluster of the same age so at current cluster ages the difference may not be as acute as initially. Furthermore, since there is a variation in total mass and velocity dispersion across the galactic globular cluster population anyway, such observations would not be conclusive in identifying two-generation clusters. A more significant and conclusive method of determining the origin of a cluster is its stellar population. Our two-generation clusters produce significantly more C-O white dwarfs than does our cluster with a Salpeter IMF and we expect these objects to be retained. Observations of white dwarf to main-sequence number ratios across the population of galactic globular clusters could determine which are two-generation candidates and may even put some limits on the number of stars in the first generation. Richer et al. (2002) find that for M4 $N_{WD}/N_{MS} \sim 1$, a fraction significantly higher than produced either by our Salpeter IMF or in our second generation clusters but approached by our top-heavy IMF. Not too much weight should be put on this at present however since our simulations end well before the current

age of the galactic globular cluster formation and will produce many more white dwarfs in their lifetimes. Again, longer simulations will provide a better comparison with the Richer et al. (2002) results. Such a count is available at present only for M4 but the deep observations necessary may soon be available for some other clusters. These stellar remnants will also be quite dark at the current globular cluster ages and their abundance may induce anomalously high mass-to-light ratios in two-generation clusters. This is an observation that could be performed across the globular cluster population to identify potential two-generation cluster candidates and would probably be easier than obtaining white dwarf to main-sequence number ratios. Indeed observations of one galactic globular cluster, NGC 6752, can already be interpreted as showing an anomalously high mass-to-light ratio possibly caused by an excess of white dwarfs in the core regions (Ferraro et al., 2003). Overall, the observations most effective at identifying two-generation cluster candidates will be those associated with the stellar population rather than the stellar dynamics.

6.3 Prospects for AGB Stars in the Self-enrichment Scenario

Our research has demonstrated that at least in the early stages of evolution two-generation clusters are as dynamically stable as their single-generation counterparts. It is worth noting that our simulations end well before the current age of the galactic globular cluster population so predictions about their state after several Gyr must be made with caution. We project, however, that such clusters could remain bound and dynamically stable for the same

length of time as their single generation counterparts (more than a Hubble time) and thus be observed as discrete dynamical objects at the current age of the universe. Thus it thus seems possible that if two-generation clusters formed at the same time as single-generation clusters, they would be included in the current population of galactic globular clusters.

We have also found that our two-generation clusters have a significantly different stellar content than those prepared according to a Salpeter formulation. In particular we expect a strong enhancement in the number of C-O white dwarfs over the Salpeter IMF clusters. This is in agreement with the predictions of D’Antona & Caloi (2004) but not in agreement with Prantzos & Charbonnel (astro-ph/0606112) who predict a smaller white dwarf to main-sequence star ratio than for a Salpeter IMF (although their scenario is slightly different). Nonetheless, a stellar population with an anomalous number of white dwarf remnants is a fixture of a second generation scenario featuring AGB stars. Since we have found no evidence that these objects will be preferentially scattered out of globular clusters, an absence of these objects would indicate they were never formed and would put restrictions on the IMF the first generation could have.

In a recent paper Karakas et al (astro-ph/0605540) consider AGB self-enrichment, examining the ability of AGB stars to produce the claimed helium enhancement in NGC 2808. They find that three reasonable AGB population models have difficulty in producing the necessary helium enhancement without violating other observations ($C + N + O \sim const.$ in this case). They conclude that AGB self-enrichment alone is insufficient to account for extreme he-

lithium enhancement in NGC 2808. Charbonnel and Prantzos (astro-ph/0606112 and astro-ph/0606220) conclude more generally that the AGB model is not favoured on the basis of IMF constraints. Another model initially proposed to describe abundances in ω Cen that is gaining some attention in the context of globular clusters places the site of self-enrichment in rotating massive stars ($> 10M_{\odot}$) which lose mass due to stellar winds and enrich the ISM on a continuing basis (Norris (2004), Maeder & Meynet (2006)). Rather than two distinct generations there is a prolonged period of star-formation with the later stars becoming progressively more enriched. This scenario may solve some of the problem with stellar remnants but only exists at a very qualitative level (Prantzos & Charbonnel, astro-ph/0606112) and needs further exploration.

6.4 Conclusion

We have investigated the dynamical implications of a scenario in which a globular cluster forms with two distinct generations, the first of which contains a top-heavy IMF and produces an excess of $\sim 3 - 5M_{\odot}$ stars. In order to confirm our results we would like to perform much longer dynamical simulation but we are able to form some preliminary and surprising conclusions. We find that a second generation cluster would be as dynamically stable over the first Gyr of its life as a single-generation cluster formed with a standard IMF. In particular, the introduction of the second generation seems to induce no dynamical instabilities in the system. We find that the dynamics of such a cluster should be indistinguishable from the single generation case but that the stellar populations should be different with the two-generation cluster en-

hanced in white dwarf stars. We conclude that although such a cluster is a dynamical possibility the overabundance of white dwarf stars and the failure of AGB stars to provide chemical enhancements matching observations make prospects for this scenario questionable at best.

Bibliography

D'Antona, F. & Caloi, V. 2004, ApJ, 611, 871

Ferraro, F. R., Possenti, A., Sabbi, E., Lagani, P., Rood, R. T., D'Amico, N.,
& Origlia, L. 2003, ApJ, 595, 179

Fukushige, T. & Heggie, D. C. 1995, MNRAS, 276, 206

Giersz, M. 2001, MNRAS, 324, 218

Hansen, B. M. S. 1999, ApJ, 520, 680

Hansen, B. M. S., Brewer, J., Fahlman, G. G., Gibson, B. K., Ibata, R.,
Limongi, M., Rich, R. M., Richer, H. B., Shara, M. M., & Stetson, P. B.
2002, ApJ, 574, L155

Joshi, K. J., Nave, C. P., & Rasio, F. A. 2001, ApJ, 550, 691

Maeder, A. & Meynet, G. 2006, A&A, 448, L37

Norris, J. E. 2004, ApJ, 612, L25

Richer, H. B., Brewer, J., Fahlman, G. G., Gibson, B. K., Hansen, B. M., Ibata,
R., Kalirai, J. S., Limongi, M., Rich, R. M., Saviane, I., Shara, M. M., &
Stetson, P. B. 2002, ApJ, 574, L151

This page intentionally left blank.